Contents lists available at ScienceDirect

Agricultural Water Management

journal homepage: www.elsevier.com/locate/agwat

Satellite-based NDVI crop coefficients and evapotranspiration with eddy covariance validation for multiple durum wheat fields in the US Southwest

Andrew N. French[a,*], Douglas J. Hunsaker[a], Charles A. Sanchez[b], Mazin Saber[b], Juan Roberto Gonzalez[b], Ray Anderson[c]

[a] USDA/ARS Maricopa, AZ, USA
[b] University of Arizona, Maricopa/Yuma, Tucson, USA
[c] USDA/ARS Riverside, CA, USA

A B S T R A C T

A three-year study was conducted to assess the ability of satellite-based vegetation index (VI) images to track evapotranspiration over wheat. While the ability of using VIs, notably with the Normalized Difference Vegetation Index (NDVI), to track vegetation growth has been well established, the operational capability to accurately estimate the crop coefficient (K_c) and crop evapotranspiration (ET_c) at farm-scale from spaceborne platforms has not been widely studied. The study evaluated wheat ET over 7 sites between 2016 and 2019 in Yuma and Maricopa, Arizona, USA estimated by using Sentinel 2 and Venus satellites to map NDVI time-series for entire wheat cropping seasons, December to June. The basal crop coefficient (K_{cb}) was modeled by the NDVI time-series and the daily FAO56 reference ET_o was obtained by near-by weather network stations. Eddy covariance (EC) stations in each field observed ET_c during the same seasonal periods, and applied irrigation amounts were logged. The experiment found that remote sensing of NDVI and modeled K_{cb} accurately estimated K_c and crop ET during mid-season through senescence in most cases. However, NDVI-based estimation performed less well during early season (< 60 days after planting), when observed ET_c was highly variable due to frequent rain and irrigation at low crop cover. Mid-season K_c values observed for the seven wheat fields were from 0.92 to 1.14, and end of season K_c values ranged from about 0.20 to 0.40, in close agreement to values reported elsewhere. Seasonal VI-based transpiration and ET_c values ranged from 467 to 618 mm, closely agreeing with seasonal EC data, which ranged 499–684 mm. Using the Venus sensor, the study in Maricopa in 2019 revealed that when augmented by a background soil water balance model, water stressed wheat can be detected mid-season with NDVI. This capability is specifically due to the sensor's ability to provide well-calibrated images every 2 days. Findings from this study will help farmers, irrigators, and water managers use and understand the capabilities of visible near infrared remote sensing to track ET_c from space.

1. Introduction

Since publication of the FAO-56 crop water requirements computational procedures (Allen et al., 1998), much research has focused on estimating crop evapotranspiration (ET_c) with real-time single (K_c) or basal crop coefficients (K_{cb}) based on vegetation index (VI) data, as applied with the FAO56 Penman-Monteith (P−M) reference-crop evapotranspiration equation (ET_o). For many annual field crops, certain biophysical parameters, such as crop-cover fraction (f_c), plant density, and leaf area index (LAI), have been closely monitored in time and space by remotely-sensed vegetation indices (Wiegand et al., 1991; Pinter et al., 2003; Duchemin et al., 2006; Hunsaker et al., 2007). For vegetation monitoring, a widely used VI is the normalized difference ratio of the near infrared (NIR) and red reflectance bands, or normalized difference vegetation index (NDVI; Glenn et al., 2011). Similarities between the time-series patterns of VIs and crop coefficients also occur, as noted decades ago by Jackson et al. (1980). Early studies by Bausch and Neale (1989) and Bausch (1995) developed methods to improve ET_c estimation for corn with the use of real-time VI-based K_{cb}, they denoted as surrogate crop coefficients. Bausch (1995) incorporated observed VI-based K_{cb} for corn within an existing weather-based irrigation scheduling model and reported reduced irrigation applications and better timing of irrigation over the model that used empirically derived time-based crop coefficients.

One of the very first studies to directly implement remotely sensed VI data within the FAO56 dual crop coefficient approach was conducted for cotton by Hunsaker et al. (2003) in Arizona, United States (US). They derived a calibration model to predict P-M-based K_{cb} with NDVI measured 2–3 times weekly using a pole-mounted radiometer over a clay loam soil. However, due to the influence of soil background on NDVI, especially soil color or brightness when f_c is low, that K_{cb}-NDVI calibration model did not transfer well when used in cotton grown in the same climate but on a sandy loam soil (Hunsaker et al., 2005a). The soil-adjusted vegetation index (SAVI) was developed by Huete (1988) to minimize soil brightness effects on spectral indices in the NIR and red wavelengths. Some research studies imply that SAVI may be a more

* Corresponding author.
E-mail address: andrew.french@usda.gov (A.N. French).

https://doi.org/10.1016/j.agwat.2020.106266
Received 1 February 2020; Received in revised form 7 May 2020; Accepted 11 May 2020
Available online 22 May 2020
0378-3774/ Published by Elsevier B.V.

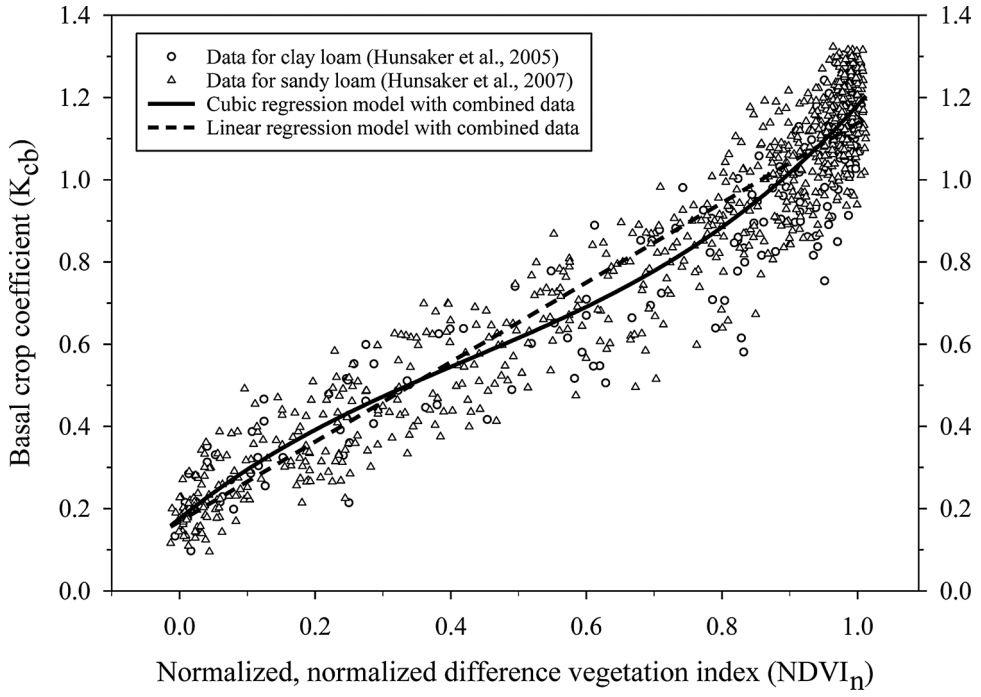

Fig. 1. Measured wheat basal crop coefficient (K_{cb}) as a function of observed normalized difference vegetation index (NDVI), normalized between 0, $NDVI_{min}$ at dry bare dry soil, and 1, $NDVI_{max}$ at full cover and resultant curves of K_{cb} by $NDVI_n$ for cubic and linear regression models.

preferable VI to model crop coefficients (Bausch, 1995; Jayanthi et al., 2007; Gonzalez-Dugo et al., 2009). While the majority of VI-K_{cb} studies to date have used NDVI, many have indirectly accounted for differences in soil background by scaling observed NDVI and K_{cb} for crops between minimum values, at dry bare soil ($NDVI_{min}$ and $K_{cb\ min}$, usually taken as 0.15), and maximum values, at effective full cover ($NDVI_{max}$ and $K_{cb\ max}$). Campos et al. (2010) compared scaled NDVI and SAVI calibration models to predict measured K_{cb} in irrigated grapes and found slightly better correlation using NDVI. Commonly, a linear relationship between K_{cb} and NDVI is assumed, as by Neale et al. (1989), Lopez-Urrea et al. (2009), Campos et al. (2010); Sánchez et al. (2012), and Rozenstein et al. (2018), and the calibration takes the form, K_{cb} = b*NDVI ± a, where a and b are the regression coefficients and NDVI is the scaled NDVI. Differently, Er-Raki et al. (2007, 2010), in Morocco, utilized a wheat K_{cb} curve using scaled NDVI as an exponential function based on LAI, thus, allowing K_{cb} to increase with NDVI in a curvilinear manner. González-Dugo and Mateos (2008) later developed a more generalized VI-based exponential model for this concept. A comprehensive listing of the many types of K_c-VI and K_{cb}-VI relationships developed for crops is provided by Pôças et al. (2020, in this Special Issue).

Assessing three-years of Maricopa, Arizona wheat field studies, Hunsaker et al. (2005b), used observed NDVI data to develop a K_{cb} model. The NDVI values were normalized between zero, for dry bare soil ($NDVI_{min}$), and 1.0, for average maximum NDVI at full cover ($NDVI_{max}$):

$$NDVI_n = [NDVI - NDVI_{min}] / [NDVI_{max} - NDVI_{min}] \quad (1)$$

where $NDVI_n$ is the normalized NDVI and NDVI is the field-observed value. Weekly measurements of wheat ET in those studies were obtained using a soil water balance (SWB), in which weekly soil water content was measured in well-watered drip-irrigated plots using neutron probe and time domain reflectometry. Average weekly values of the K_{cb} were calculated by the FAO56 dual approach based on the FAO56 P-M ET_o equation using meteorological parameters measured by the University of Arizona weather station at Maricopa. The weekly K_{cb} values were paired with average weekly $NDVI_n$ measured with a pole-mounted radiometer above the plots. In that clay loam soil field, the average observed $NDVI_{min}$ by the radiometer varied from 0.155 to 0.191 for the three years, whereas the average maximum NDVI only varied from 0.922 to 0.927. The relationship between K_{cb} and $NDVI_n$ was found to be described by a cubic regression model with a coefficient of determination (r^2) of 0.90, n = 232 (Hunsaker et al., 2005b). The model was then applied in real-time irrigation scheduling studies for two years with the same wheat variety at a nearby site in Maricopa that had sandy loam texture at the soil surface and sandy clay loam texture at deeper layers (Hunsaker et al., 2007). Using the same radiometer methods as in the clay loam studies, $NDVI_{min}$ values measured for dry bare soil were on the order of 0.10 − 0.11 for the sandy loam, while $NDVI_{max}$ was assumed as 0.925 (based on that observed in the clay loam). For real-time use in irrigation scheduling, prior knowledge of $NDVI_{max}$ for a crop is needed in order to properly scale the time-series $NDVI_n$ to K_{cb}. However, when different platforms and sensors are used for NDVI, $NDVI_{max}$ values for a given crop will likely vary depending on the sensor configuration and atmospheric correction techniques used. Thus, empirical observations of $NDVI_{max}$ for the given crop and sensor system are recommended before the VI method is used in irrigation scheduling. During the first year in the study by Hunsaker et al. (2007), the assumed $NDVI_{max}$ was very close to that measured at full cover (0.92 − 0.93) for well-watered and -fertilized wheat and K_{cb} wheat ET predictions versus measured, as derived from the SWB, were highly correlated (r^2 = 0.94 − 0.95). Although measured $NDVI_{max}$ was lower in the second year (0.89 − 0.91) due to nitrogen stress during crop development, the ET_c predicted by the K_{cb}-$NDVI_n$ model remained highly correlated with the measured ET_c (r^2 = 0.88 − 0.94), indicating that the predictions of K_{cb} based on $NDVI_n$ were appropriate for the non-optimal crop conditions as well as for optimal conditions (Hunsaker et al., 2007). With the abundance of K_{cb}-$NDVI_n$ data collected in the sandy loam wheat studies, the data were combined with the data from the clay loam field to upgrade the wheat cubic regression model (Fig. 1). A comparison of the derived cubic model with a linear model for wheat shows that K_{cb} varies with $NDVI_n$ in three phases. For low $NDVI_n$, between 0 and 0.4 (emergence to about 25% cover), K_{cb} increases linearly with $NDVI_n$. As crop development continues (i.e., as

Table 1
Regression coefficients and statistics for wheat basal crop coefficient (K_{cb}) as a cubic function of the normalized, normalized difference vegetation index ($NDVI_n$) using data from Hunsaker et al. (2005 and 2007).

Regression coefficients[a]				Regression statistics[b]		
a0	a1	a2	a3	r^2	se	n
0.176	1.325	−1.466	1.146	0.924	0.097	991

[a] $K_{cb} = a0 + a1X + a2X^2 + a3X^3$, where X is $NDVI_n$.
[b] r^2 is the coefficient of determination, se is the standard error of the estimated K_{cb}, and n is the sample size.

$NDVI_n$ goes from 0.40 to 0.90), the rate increase of K_{cb} is less than the linear model. This occurs as f_c increases from 25% to about 75%. In the third phase, between $NDVI_n$ from 0.90 to 1.0 (75–100% cover), K_{cb} increases more rapidly than $NDVI_n$. These different trends in K_{cb} versus $NDVI_n$ for wheat could also be modeled by three segmented linear regression lines. However, the third-order regression model captures the variations well and is easier to compute. The regression coefficients and related statistics for the cubic model of Fig. 1 are given in Table 1.

The subject for this VI study, durum wheat (*Triticum turgidum* ssp. *durum* Desf.), also called pasta wheat, is one of the most important crops grown worldwide (Kabbaj et al., 2017). It is also one of the primary crops produced in irrigated desert regions of the southwestern US, including Arizona and California. Desert durum is grown as a winter crop in the state of Arizona, which has become the third largest producer of durum wheat in the US (Mon et al., 2016). Yuma County, situated in the low desert of southwestern Arizona, is one of the world's foremost producers of lettuce and other winter vegetables. However, cultivation practices in the area are dominated by rotational cropping systems, where a winter vegetable crop is followed by durum wheat, melon, or short-season cotton (Taylor and Koo, 2015). Desert durum, in particular, when grown in rotation, plays an important secondary role in providing soil health benefits, including maintaining soil salinity at optimal levels for the next vegetable crop.

A continuous goal in Yuma and other irrigated desert areas in Arizona is obtaining high crop productivity and reducing water use through improved management practices. Most of the gains in increased irrigation water use efficiencies in recent years for Yuma have

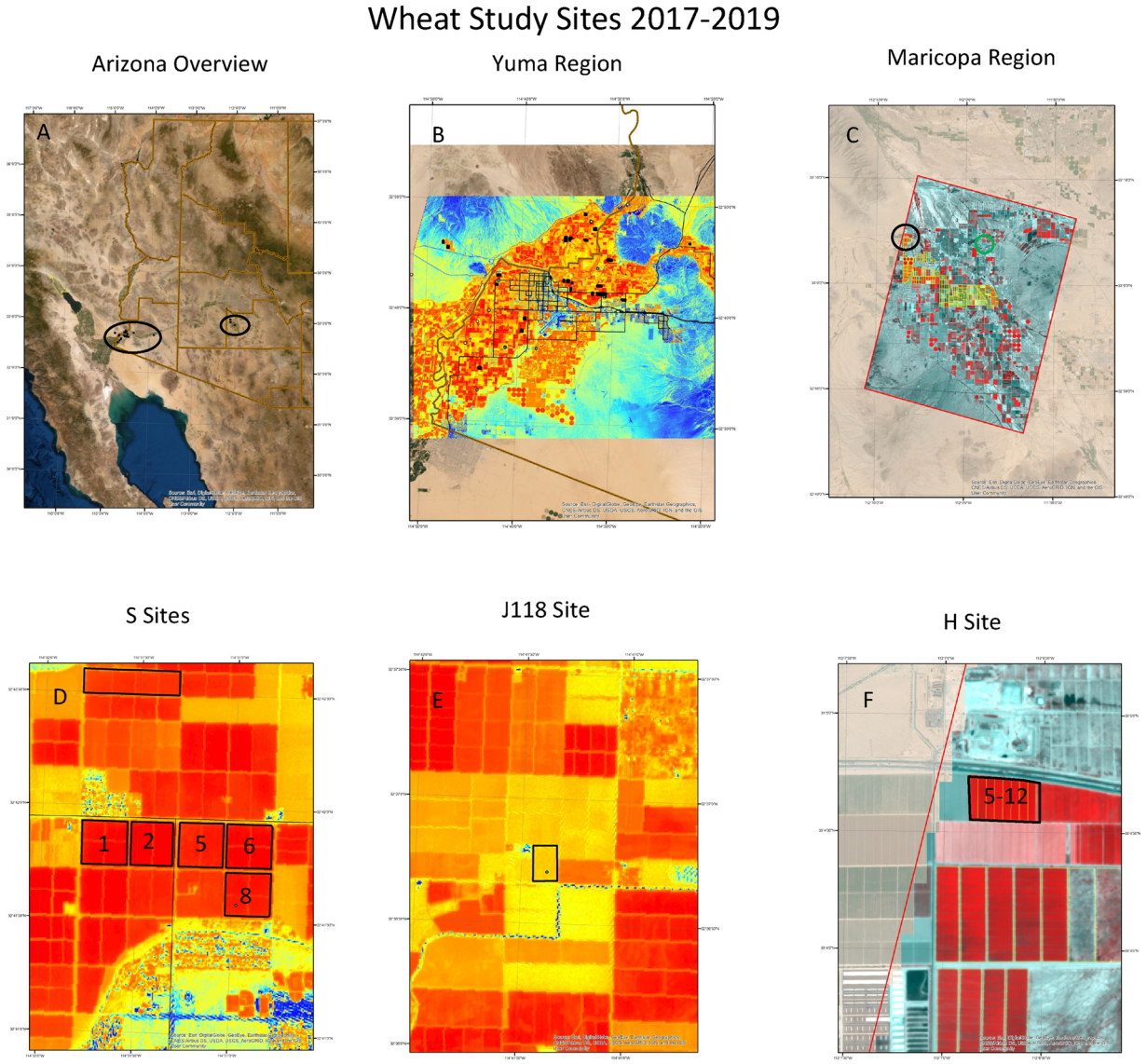

Fig. 2. Arizona wheat site locations. Synoptic view of southern Arizona, with Yuma and Maricopa sites, separated by ~240 km, are outlined in black (A). Regional view of Yuma, ~35 km x 35 km, with false-color NDVI from Sentinel 2 (B) Red colors indicate dense green vegetation, yellow, green, and blue colors indicate sparse cover. Regional view of Maricopa, district width ~18 km, with false-color NDVI from Venus (C). Site specific maps are shown for Yuma S1, S2, S5, S6, and S8, fields 360 m east-west (D), Yuma site J118, 180 m east-west (E), and Maricopa H borders 5-12, total width 520 m east-west (F). (For interpretation of the references to color in this figure legend, the reader is referred to the web version of this article.)

been attributed to on-farm infrastructure improvements, precision land leveling, and minimizing crop production during the high evaporative demand months of summer (Taylor and Koo, 2015). Improved irrigation scheduling methods could also play an important role in boosting water use efficiencies. While most growers are aware of crop coefficient methods for irrigation scheduling, they are not widely used. In addition, the available wheat crop coefficients for Yuma and other Arizona counties, which were developed years ago, need to be re-evaluated and updated. Nevertheless, most growers of durum wheat in these areas are highly experienced irrigators, though usually relying primarily on soil shovel turning to estimate soil water depletion (Taylor and Koo, 2015).

To date, operational applications of K_{cb}-VI approaches for crop ET monitoring and irrigation management in the US Southwest have not been extended much beyond research studies. Thus, the derived K_{cb}-$NDVI_n$ model for wheat described in Table 1 has not yet been evaluated at the farm scale. But the rising number of public earth observation systems, particularly the Sentinel 2 mission and the new microsatellite, Venus (theia.cnes.fr), makes an evaluation in irrigated fields feasible. Sentinel 2 data can provide an NDVI time-series at high temporal (every five days) and spatial resolution (≈10 m; Transon et al., 2018; Rozenstein et al., 2018). Venus has similar spectral characteristics to Sentinel 2 but with 5 m nadir resolution, and 2-day, constant view-angle acquisitions. Therefore, to provide a starting point towards improved irrigation scheduling for durum wheat in the US Southwest, studies were conducted to evaluate the K_{cb}-$NDVI_n$ model in seven commercial durum wheat farms, six in Yuma County and one at Maricopa in Pinal County, Arizona. Study objectives were (1) to assess model-estimated crop transpiration (T_c) and crop ET using Sentinel 2 and Venus NDVI time-series data in comparison with measured daily crop ET obtained by eddy covariance (EC) towers installed at each field site; (2) to derive single K_c values for durum wheat based on measured ET_c and the FAO56 P-M ET_o; and (3) to evaluate cumulative seasonal irrigation applied at each site with respect to the measured and estimated seasonal ET_c.

2. Methods

2.1. Study sites

The durum wheat sites were in Southern Arizona (Fig. 2A), hot and arid lands receiving little rainfall, typically ranging from 80 mm to 200 mm annually from western to central parts of the State. This means that irrigation is required for all crop production. Most irrigation is applied by gravity in level basins and borders. The study included 6 commercial sites in the Yuma region (Fig. 2B) and one commercial site in the Maricopa region (Fig. 2C), 81,000 and 23,800 irrigated hectares, respectively. All were level-basin irrigated. In recent years the Yuma district has used approximately 108,000 ha-m of Colorado River water. The Maricopa-Stanfield Irrigation District uses approximately 37,000 ha-m of co-mingled ground and Colorado River water.

The six sites in Yuma were on private farms, denoted as S1, S2, S5, S6, S8, J118 (Fig. 2D and E). The seventh site in Maricopa was also on a private farm (H8, Fig. 2E). General site descriptions are shown in Table 2, providing planting/harvest dates and length of run for the irrigation borders. Reference weather data were taken from the AZMET system (cals.arizona.edu/AZMET), which provides data over grass reference surfaces. Table 3 shows the average monthly data for weather parameters for the Gila North Yuma AZMET station, located approximately 8–12 km north of the Yuma sites. Table 4 provides the average weather data for the Maricopa Agricultural Center station, about 8 km east of the H8 site. Soil texture fractions were measured from samples taken in the top 0.15 m soil depth at each site (Table 5) using a Laser Diffraction Particle Size Analyzer. All sites were part of crop rotations, with double cropping of leafy greens and wheat common for Yuma fields.

Table 2
Planting and harvest dates and length of irrigation borders for seven monitored durum wheat field sites in Yuma and Maricopa, Arizona*.

Site	Year	Location	Plant date	Harvest date	Length of run (m)
S8	2016 – 17	Yuma	Dec. 18	May 5	381
J118	2017	Yuma	Jan. 11	Jun. 1	273
S1	2018	Yuma	Jan. 5	May 31	392
S2	2018	Yuma	Jan. 6	May 31	385
S5	2017 – 18	Yuma	Dec. 15	Jun. 1	382
S6	2018	Yuma	Jan. 24	Jun. 1	383
H8	2018 – 19	Maricopa	Dec. 18	May 25	360

* All wheat fields were irrigated in borders (flood).

2.2. Evapotranspiration measurements

The field schedule for evapotranspiration measurements consisted of eddy covariance stations as listed in Table 6. The station components (Table 7) were predominantly manufactured by Campbell Scientific (Logan, UT), but also included LI – COR (Lincoln, NE) infrared gas analyzers, Kipp & Zonen net radiometers (Delft, Netherlands), Hukseflux soil heat flux plates (Delft, Netherlands), and Vaisala HMP45 temperature humidity probes (Vantaa, Finland). Five unique stations were used for the study, 3 of which were new instruments (2017). Station contributors were University of Arizona/YCEDA (1), USDA/ARS Maricopa (2), and NASA/JPL (2). All loggers (CR3000, Campbell Scientific) and covariance sensors were calibrated by the manufacturer in 2016 and 2017. Zero and span of infrared gas analyzers (IRGA) were done in July 2017 and again in July 2018. Stations were deployed immediately after planting, then removed just prior to harvest. Occasionally stations had to be moved mid-season to allow farm equipment access for spray applications. In these instances, the EC and net radiometers were temporarily relocated while the soil heat flux plates remained in place. On re-entry, the sensors were replaced within a few cm of their original locations. Each station included an EC, IRGA, net radiometer, at least two soil heat flux plates, logger, cell modem, and solar power supply. ECs were set horizontally- all sites were flat and close to level- and mounted approximately 1 m above the top of canopy. Net radiometers were deployed 1 m over the canopy and facing due south. With two exceptions two soil heat flux plates were deployed adjacent (i.e.- offset 1 m east and west) to the station's net radiometer and at 5 cm depths. The exceptions were at S8 and J188 sites where four plates were deployed. To estimate heat storage above the plates, two pairs of thermocouples were installed above each plate. One soil moisture sensor, CS616 (Campbell Scientific), was installed midway between plates at 5 cm depth. Note however that the net storage at daily time steps was small and was not included in the energy budgets. Each EC assembly was raised during the season as needed to maintain a minimum 1 m offset. EC azimuths were set due south at S8 and J118, and due west at S1, S2, S5, S6, and H8 to reduce instances of self-obstructed airflow: predominant winds were from the western half of the compass at Yuma and from the south at Maricopa.

Each station collected multiple micrometeorological observations (~108 variables per time step) at 20 Hz sample rates, configured under Campbell Scientific's EasyFlux DL ™ (Logan, UT) program[1] to allow continuous data measurements during the cropping cycle. Simultaneously 30-min block-averaged fluxes, including the Webb-Pearman-Leuning (Webb et al., 1980) corrections were stored. Computation of 30-min evapotranspiration (ET) estimates used WPL fluxes. EC stations, with few exceptions, were visited weekly to inspect horizontal and azimuthal alignment, cleared of bird debris, and general operation. Station functioning was monitored daily via cell-phone modem links.

[1] Mention of tradenames and commercial products is for reader convenience and does not imply endorsement. USDA does not endorse or recommend products.

Table 3
Monthly average weather parameters; maximum (T_{max}) and minimum daily (T_{min}) temperatures, minimum relative humidity (RH_{min}), solar radiation, 2-meter wind speed, growing degree day (GDD), reference evapotranspiration (ET_o), and monthly total rain as recorded from December 2016 through May 2018 at the Gila North Yuma AZMET station.

		Monthly daily means							Monthly total
Year	Month	Tmax (°C)	Tmin (°C)	RHmin (%)	Sol. Rad. (MJ/m^2)	2-m wind (m/s)	GDD (°C-d)	ETo (mm/d)	Rain (mm)
2016	Dec.	20.1	5.9	31.1	11.1	1.9	8.4	2.2	19.3
2017	Jan.	19.6	5.6	33.6	11.6	2.1	8.2	2.4	6.6
	Feb.	24.0	8.9	29.5	15.0	1.8	12.0	3.0	34.0
	Mar.	29.4	10.4	15.1	21.9	1.9	15.2	4.9	3.0
	April	31.6	12.3	11.4	26.1	2.0	17.0	6.3	0.0
	May	33.9	14.3	14.8	28.7	1.9	18.7	6.9	3.0
	Dec.	22.2	4.9	15.5	12.3	2.0	9.2	2.8	0.0
2018	Jan.	23.8	6.2	19.9	13.2	1.8	10.6	2.9	4.0
	Feb.	23.2	4.9	17.7	16.7	1.7	9.7	3.2	0.0
	Mar.	26.3	9.0	14.9	20.5	1.9	13.2	4.5	0.0
	April	32.0	12.6	11.3	25.5	2.0	17.5	6.3	0.0
	May	33.6	13.9	13.7	29.6	1.8	18.7	6.9	0.0

Table 4
Monthly average weather parameters; maximum (T_{max}) and minimum daily (T_{min}) temperatures, minimum relative humidity (RH_{min}), solar radiation, 2-meter wind speed, growing degree day (GDD), and reference evapotranspiration (ET_o), and monthly total rain as recorded from December 2018 through May 2019 at the Maricopa Agricultural Center AZMET station.

		Monthly daily means							Monthly total
Year	Month	Tmax (°C)	Tmin (°C)	RHmin (%)	Sol. Rad. (MJ/m^2)	2-m wind (m/s)	GDD (°C-d)	ETo (mm/d)	Rain (mm)
2018	Dec.	18.6	2.2	29.3	10.6	1.3	6.3	1.8	14.0
2019	Jan.	18.7	2.7	32.5	12.4	1.3	6.6	1.9	13.0
	Feb.	16.8	3.5	31.3	14.4	1.8	6.3	2.4	63.0
	Mar.	24.5	7.4	19.2	20.4	1.9	11.5	4.2	7.0
	April	30.5	12.8	12.6	25.7	2.3	16.9	6.5	0.0
	May	30.6	14.2	13.6	27.7	2.4	17.8	7.0	0.0

Table 5
Soil texture characteristics for the 0-0.15 m soil depth measured at the seven monitored durum wheat field sites in Yuma and Maricopa, Arizona.

Site	Year	Clay (%)	Silt (%)	Sand (%)	USDA Soil Texture
S8	2016−17	21.7	40.0	38.4	Loam
J118	2017	18.1	21.4	58.4	Sandy loam
S1	2018	24.3	57.0	18.7	Silt loam
S2	2018	23.7	43.3	33.1	Loam
S5	2017−18	22.9	43.4	33.7	Loam
S6	2018	23.8	36.5	39.7	Loam
H8	2018−19	29.2	20.2	50.6	Sandy clay loam

Table 6
Wheat eddy covariance site schedules and reference weather stations.

Site	Region	Area (ha)	Location	Elev. (m)	Owner/ID	Deploy	Remove
S8	Yuma	129.13	32° 41′ 37″ N; 114° 30′ 51″ W	46	USDA 1	14 Dec 2016	5 May 2017
J118	Yuma	46.96	32° 36′ 45″ N; 114° 41′ 23″ W	34	USDA 2	12 Jan 2017	1 Jun 2017
S5	Yuma	129.67	32° 41′ 51″ N; 114° 31′ 10″ W	45	JPL 1	18 Dec 2017	1 Jun 2018
S1	Yuma	131.02	32° 41′ 50″ N; 114° 31′ 41″ W	45	USDA 1	5 Jan 2018	31 May 2018
S2	Yuma	119.74	32° 41′ 51″ N; 114° 31′ 26″ W	45	JPL 2	8 Jan 2018	31 May 2018
S6	Yuma	130.68	32° 41′ 50″ N; 114° 30′ 56″	46	USDA 2	29 Jan 2018	1 Jun 2018
H8	Maricopa	247.40	33° 4′ 39″ N; 112° 6′ 43″ W	355	UA 1	18 Dec 2018	24 May 2019
AZMET: Yuma North Gila	Yuma		32° 44′7″ N, 114° 31′ 49″ W	45		1 Jan 1987	–
AZMET: Maricopa	Maricopa		33° 04′ 8″ N, 111° 58′ 20″ W	362		22 Jan 1988	–

Data were stored on Compact Flash (CF) cards that were changed approximately every 2 weeks.

Subsequent processing of fluxes used R scripts to remove data spikes and fill data gaps. Spike removal followed the methodology described by Vickers and Mahrt, 1996. Gap filling was needed to avoid underestimation of ET. The nature of the gaps varied for station and site and, except for station relocations, were unpredictable. Sometimes the IRGA would fail but not the sonic, other times both failed, and on still other occasions inexplicably self-resolved. Gap-filling techniques have been reported in reviewed in literature, e.g., 15 of them by Moffat et al. (2007). The best approach would be to adopt one or more of those, but time did not allow testing and implementation for all sensor and data collection maladies. Hence linear interpolation of relevant and co-variant variables was employed where feasible, meaning that fluxes were reconstructed from fundamental observables such as wind speed, air temperature and humidity if available from ancillary instruments. For example, when the IRGA failed but not the sonic, H fluxes were estimated by computing air density and heat capacity via independent slow-response temperature humidity sensors. For long-duration time gaps, more than 2 h, linear interpolation to 30-minute time steps was not done and an alternative strategy had to be used. In these cases, gap

Table 7
Eddy covariance instrumentation.

Name	Deployment Sites	Covariance Sensors	Net Radiometer	Soil Heat Flux Plates
ALARC1	S8, S1	CSAT3, LI7500	REBS Q7	Hukseflux Self-Calibrating
ALARC2	J118, S6	CAT3, LI7500	REBS Q7	Hukseflux Self-Calibrating
JPL1	S5	EC150	Kipp & Zonen CNR4	Hukseflux
JPL2	S2	EC150	Kipp & Zonen CNR4	Hukseflux
UA1	H8	Irgason	NRLite	Hukseflux

filling was done daily since variability at shorter time steps was high. Energy balance closure was enforced using the Bowen ratio method (Eq. (2), Twine et al., 2000):

$$LE_{corr} = (R_n\text{-}G)/(\beta + 1) \quad (2)$$

where LE_{corr} is the closure corrected latent heat flux, R_n is net radiation, G is soil heat flux, and β is the Bowen ratio (sensible heat flux, H, divided by observed latent heat flux, LE). Observed daily ET, ET_c, (mm) was then computed by summing 30-minute, LE_{corr} samples:

$$ET_c = \sum_{n=1}^{48} \frac{LE_{corr,n}}{\lambda_{v,n}\rho_{w,n}} \quad (3)$$

where n is a 30-minute time sampling index, λ_v is latent heat of water vaporization (J/kg) and ρ_w is water density (kg/m^3).EC data quality was further evaluated using energy balance closure estimation following similar procedures (metabolic storage was omitted) to those described in Anderson and Wang (2014). Closure is the ratio of eddy covariance available energy (AE_{EC} = H + LE) to the so-called 'radiometric' available energy (AE_{RAD} = R_n - G):

$$Closure = \sum_{n=1}^{48} \frac{AE_{EC}}{AE_{RAD}} \quad (4)$$

2.3. Satellite observations

Data required for this study were calibrated, multispectral visible near infrared reflectance data with high spatial resolution (20 m or better) and high temporal frequencies (weekly or better). Multispectral data were needed to create vegetation indices, critically NDVI ([NIR-Red]/[NIR + Red]) from red (~670 nm) and near infrared (~800 nm) reflectance. High spatial resolution was needed to resolve wheat fields without significant field-edge effects. High temporal frequencies were needed track the rapidly changing wheat canopy and to maintain good time resolution despite cloudy sky events. Data from two satellite sensors (Table 8) met these requirements: Sentinel 2 a/b, (www.esa.int/Applications/Observing_the_Earth/Copernicus/Sentinel-2) for 2017 and 2018 Yuma data, and Venus (https://www.theia-land.fr/en/product/venus/) for the 2019 Maricopa data. Incorporation of additional observations from Landsat 7 and 8 would improve temporal sampling. However, they were not included due to the need for additional analyses to accommodate coarser (30 m) spatial resolution and similar, but not identical, spectral sampling. These differences complicate the generation of a unified NDVI time-series.

Table 8
Remote sensing satellite acquisition attributes for the Sentinel 2 and Venus sensors. Counts denote total number of scenes acquired and used in this study.

Sensor Attributes	Sentinel 2 a/b	Venus
Resolution (m)	10 – 20-60	5 – 10
Overpass time (MST)	~11:25	~11:28
Overpass frequency (day)	5	2
Swath width (km)	290	27
Number of bands	13	12
NDVI bands	B4: 665 nm; B8: 842 nm	B7: 667 nm; B11: 865 nm
Image format	JPEG2000, 1 file per band	GeoTIFF, 1 file for all bands
Scenes: Yuma 2017	25	–
Scenes: Yuma 2018	58	–
Scenes: Maricopa 2019	–	65

Sentinel 2 (a/b) is a pair of identical satellites collectively observing identical targets weekly. They are multispectral pushbroom instruments in sun-synchronous orbits with overpass times in Arizona at ~11AM. Data for NDVI have 10 m resolution. Orthorectified, 100 km x 100 km tiles, with top-of-atmosphere (TOA) reflectance (L1C), were downloaded from USGS (earthexplorer.usgs.gov). Because UTM zone 12 is used for all Arizona sites as part of USDA Maricopa lab GIS protocol, Yuma area images needed to be re-projected: Yuma lies slightly west of the nominal zone 12 boundary of 114°W. For this task the GDAL (gdal.org) package gdalwarp, as implemented in rgdal, was used. Sentinel 2 NDVI values were generated from top of atmosphere (TOA) bands 4 and 8.

Atmospherically corrected reflectance data are generally preferred—and were used for the Venus sensor data as noted below– because the resulting indices are more representative of actual vegetation conditions than those derived from uncorrected data. This preference, however, created a difficult-to-resolve data processing challenge. Tools such as 6S, Sen2Agri, and MAJA- a package combining the Multi-sensor Atmospheric Correction and Cloud Screening (MACCS) and ATCOR (Hagolle et al., 2015)- could have been used, but necessary local atmospheric data and computer hardware were not available. For consistency, this unavailability suggested that all analyses be conducted using less-than-optimal TOA data. On the other hand, if the effects of atmospheric corrections upon ET estimates could be quantified, then a compromise could be made. TOA data could be included while not losing results where surface reflectance data were available.

To show the viability of this latter approach, we evaluated the effects of atmospheric corrections on four key parameters: NDVI, $NDVI_n$ (Eq. (1)), K_{cb}, and ET_c using 'Venus' (theia.cnes.fr) data. The Venus project enabled the evaluation since it provides both 5-m top-of-atmosphere reflectance (L1C) and MAJA-generated 10-m surface reflectance (L2A) data. Two regions from 2019 were considered: the Maricopa wheat field H8 and Yuma wheat fields S1, S2, S5, S6, and S8. Note that wheat grown at Yuma in 2019 was not part of the ground study, which meant that ET_c estimates from the atmospheric comparison study were compared but not validated. The full wheat season, late December 2018 to early June 2019 were assessed with 49 scenes over Maricopa and 79 over Yuma. We show below that use of top-of-atmosphere data—filtered to include only scenes with no visible clouds–introduces small (<5%) bias errors.

For wheat grown in 2019 at Maricopa, Venus microsatellite data were used (data not available over Yuma for the 2018 sites). Venus (Table 8) has similar spectral responses to Sentinel 2 but is superior in several ways: higher spatial resolution- 5 – 10 m nadir resolution vs. 20 – 60 m, 2-day, constant view-angle acquisitions vs. 5 – 10-day overpass frequency, and availability of both top-of-atmosphere and atmospherically corrected reflectances. Consequently, the potential temporal sampling intervals were greatly improved over alternative sensors. Orthorectified, 27 km x 27 km, multispectral L2A, 10 m surface

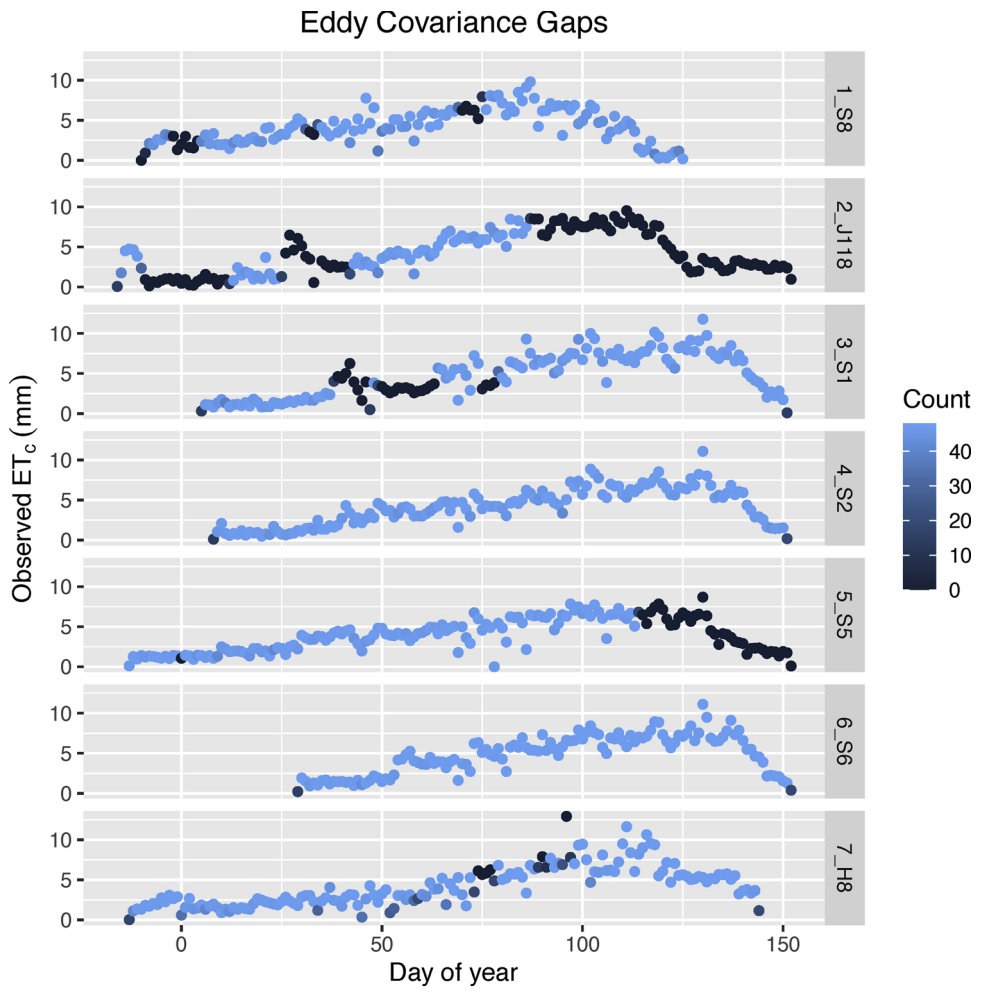

Fig. 3. Eddy covariance daily data gap. Observed daily ET_c from the seven sites are shown by their corresponding day of year. Daily observations with no gaps, 48 samples (from 30-minute time averages) are coded blue. Observations with gaps are coded with progressively darker gray values as the valid sample counts decrease. S2, S6, and H8 sites had the fewest gaps, while J118 had the greatest. S5 was mostly gap-free except for the final 30 days of the 2018 experiment. (For interpretation of the references to color in this figure legend, the reader is referred to the web version of this article.)

reflectance, were used.

Having noted a preference for atmospherically corrected reflectance images, it also needs to be noted their use introduces a different side-effect: high sensitivity to noise in the red band. Since healthy vegetation has very low reflectivity in the red band, noise in this spectral region can leadto anomalously high NDVI values. One compensation approach for this outcome is to apply a constant offset to the red reflectance (Hagolle, et al., 2015, labo.obs-mip.fr/multitemp/using-ndvi-with-atmospherically-corrected-data/), to create a revised 'NDVI' denoted ACORVI:

$$\text{ACORVI} = [\text{NIR}-(\text{Red}+0.05)]/[\text{NIR}+(\text{Red}+0.05)] \quad (5)$$

The suggested offset, 0.05, is chosen to be small, yet greater than the standard deviation of atmospheric correction uncertainty, typically ~0.01. This study used Eq. 5 for all Venus-acquisitions but report them as NDVI below.

2.4. Estimation of transpiration and evapotranspiration using vegetation indices

We use the empirical Vegetation Index for the Southwestern US (VISW; French et al., 2018) to transform remotely sensed reflectance maps into daily evapotranspiration. VISW uses NDVI as a proxy for the basal crop coefficient, K_{cb}. Thus, instead of using standardized estimates of vegetation cover, one uses observations from satellite or airborne images and an empirical transformation developed by Hunsaker et al. 2005b; and 2007 (Fig.1, Table 1), i.e.:

$$K_{cb} = \min [0.15;\ 0.176 + 1.325\ \text{NDVI}_n - 1.466\ \text{NDVI}_n^2 + 1.146\ \text{NDVI}_n^3] \quad (6)$$

where NDVI_n is normalized NDVI as calculated in Eq. (1).

For the present study, the NDVI_{min} and NDVI_{max} values used to estimate the K_{cb} for field sites are the lower and upper NDVI limits. Rigorous criteria for optimal limit selection do not exist, hence objective thresholds based on observations were used: we selected probability levels of 10% and 90% from the empirical NDVI distributions. As defined in FAO56, when potential effects of water stress on ET_c are considered, actual ET_c ($ET_{c\ act}$) is computed as:

$$ET_{c\ act} = (K_s\ K_{cb} + K_e)\ ET_o \quad (7)$$

where K_{cb} represents crop transpiration (T_c), K_e is a coefficient for soil evaporation, K_s is the water stress coefficient, and ET_o is grass reference evapotranspiration. For the Yuma sites, we limit evaluation of the model (Equation 5 above) to only estimate K_{cb} with satellite NDVI, and thus, calculate only the T_c portion of ET_c, that is, K_{cb} times ET_o. K_s was not computed but assumed as 1.0 since we did not model the soil water balance (SWB). Thus, water stress, if any, was not accounted for in the Yuma T_c estimates. However, for the Maricopa field (H8), having more

frequent NDVI acquisitions, simulated daily SWB estimates, i.e., a separate root zone and surface soil layer SWB, were made. These enabled estimation of actual ET_c by evaluating K_e and K_s using the FAO56 dual crop coefficient procedures. Parameters for calculating K_e were based on the soil evaporation characteristics given in FAO56 for the sandy clay loam soil at H8. Fraction of soil wetted by irrigation and precipitation was set to 1.0. Crop height and crop rooting depth were increased proportionately with estimated K_{cb} until maximum values of 0.90 and 1.5 m, respectively, were reached, maximum values referred to in FAO56 for wheat. Similarly, crop cover was increased to a maximum of 0.99 at maximum K_{cb} but was allowed to decrease proportionately with K_{cb} during late season senescence. The soil water depletion fraction for no water stress (p) was set to 0.55 for $ET_{c\ act}$ = 5.0 mm day^{-1}, and adjusted daily for atmospheric demand, per FAO56, Table 22, and footnote 2. In computation, $K_s = TAW - D_r / (1-p)\ TAW$, where TAW is total available water in the root zone (mm) and D_r is the root zone depletion (mm).

Statistical comparisons between daily observed ET_c and either T_c (S sites) or $ET_{c\ act}$ (H site) were evaluated separately over different growth stages, as well as for the entire wheat season. Growth stages were estimated based on evaluation of seasonal observed K_c tends, as described in the next section. For each site, statistics were analyzed over the initial and development, mid-season, and late season stages. Analyses included linear correlation and root mean square error (RMSE), mean difference (MD), mean absolute difference (MAD), and percent MAD (MADP) relative to the observed mean.

2.5. Measured and estimated crop coefficients

Daily values of the single crop coefficient, K_c, were calculated for sites by dividing the observed daily ET_c from eddy covariance by daily ET_o. Segmented, linear FAO56 K_c curves were derived by visually fitting the K_c data to the initial, mid-season, and late season growth stages. The model estimated K_{cb} for the Yuma sites and the K_{cb} and K_c (H8 site only) were compared to the observed K_c.

2.6. Evapotranspiration terminology

To summarize, this study compared evapotranspiration estimates from eddy covariance stations – denoted 'observed ETc '– against vegetation index-based estimates derived from satellites in two different ways. For all Yuma sites, model estimates represent just the transpiration component of ET_c and are denoted as 'T_c '. For the Maricopa site (H8), modeling incorporated a soil water balance and results there are indicated as '$ET_{c\ act}$'.

3. Results

3.1. Daily eddy covariance ET_c and ET_o

Eddy covariance data from all seven sites were quality checked- unrealistic values were removed, time data gaps filled, energy balance enforced- then outputs were compared with ET_o.

Daily observed ET_c plots (Fig. 3) display the timing of data gaps in terms of sample counts, where non-gap days (over 48, 30-minute samples) are shown in blue. Continuously gapped days (0 samples) are in black. Three of the sites (S2, S6, and H8) had few gaps and could mostly be filled by linear interpolation. The other four sites (S8, J118, S1, and S5) had longer duration gaps and required multiple correction procedures. Gaps at S8 and S5 were almost exclusively due to loss of IRGA, but not sonic values; for these, missing LE data were estimated by energy balance residuals. Gap-filling at S1 was done by a fortuitous arrangement with S2, an adjacent site with the same planting date and similar irrigation history. In this case, linear regressions between the S1 and S2 flux components during non-gapped times were used to create predictions to fill S1 gaps. The J118 site was the most problematic case. Three different procedures were needed to fill gaps: linear interpolation was done for gaps less than 2 h, LE fluxes were computed by residuals for early and mid-season times, while for late times gap filling was done only at daily time intervals and used estimated crop coefficients. This last step was done by using AZMET Yuma North Gila ET_o values, computing K_c at the bounds of the data gap, and then linearly interpolating the product, K_c x ET_o.

Closure was computed for all stations at daily time steps, a procedure that reduces energy storage effects, then fit with linear models. Reported in Table 9 are the summary statistics for each site on the left half, and cumulative monthly (Feb-May) observed ET_c (mm) before and after correction via Eq. (2). Average monthly observed ET_c error, considering all months (Dec-Jun), was 37 mm, which means that closure-corrected cumulative observed ET_c values were ~30% greater than uncorrected observations.

Eddy covariance data over wheat for all three years showed consistent patterns of early season observed ET_c at 1 mm/day ramping up to over 8 mm/day mid-season, then rapidly dropping to < 1 mm/day on senescence. Comparisons between observed ET_c, which includes both vegetation transpiration and soil evaporation and weather station derived ET_o, are shown for all 7 sites in Fig. 4 for 2017, Fig. 5 for 2018, and Fig. 6 for 2019, where solid symbols indicate observed ET_c from eddy covariance observations and open symbols represent ET_o calculated from Yuma North Gila and Maricopa AZMET stations. Observed ET_c usually falls below ET_o until DOY 60, then closely tracks it for the remainder of the season until senescence. Spikes in observed ET_c of 2.0 or more mm/day above the trend generally coincide with preceding irrigation or precipitation events (also shown in Figs. 4–6). Most notable for high observed ET_c to ET_o ratios during early season were the S8 site in Yuma (2016−17; Fig. 4a) and the H8 site in Maricopa (2018−19; Fig. 6). Both sites in their respective wheat years experienced an irrigation immediately after planting and significantly more precipitation events early in the wheat season as compared to other sites and years. Cumulative observed ET_c ranged from 499 mm to 684 mm (Table 10).

Table 9
Evapotranspiration closure assessment at monthly intervals for the 2017-2019 wheat studies. Linear model statistics- R^2, RMSE (W m^{-2}), number of days (N), were derived from non-gap-filled observations of AEEC vs. AERN. ET values are shown by month before and after energy balance closure corrections for February-May. With exceptions for sites S2 and S6, total corrected ET_c values are less than reported in Table 10 because gap interval estimates are not included.

Site	R^2	RMSE W m^2	N	ET_c (mm $month^{-1}$)			
				Feb	Mar	Apr	May
S8	0.61	30	119	64.8/107.9	95.5/166.2	33.7/129.0	2.2/6.2
J118	0.63	28	51	35.3/57.5	102.6/179.7	-/82.5	-/73.5
S1	0.94	12	113	-/16.1	91.9/109.1	-/198.5	-/164.4
S2	0.92	12	140	55.0/80.3	104.3/135.6	160.6/192.8	138.3/156.9
S5	0.83	17	123	67.3/130.3	104.4/174.6	116.5/177.3	-/-
S6	0.95	8	120	39.8/63.6	109.7/138.6	166.5/197.4	154.1/172.4
H8	0.71	24	141	50.5/72.0	77.2/108.5	149.9/201.3	98.1/118.0

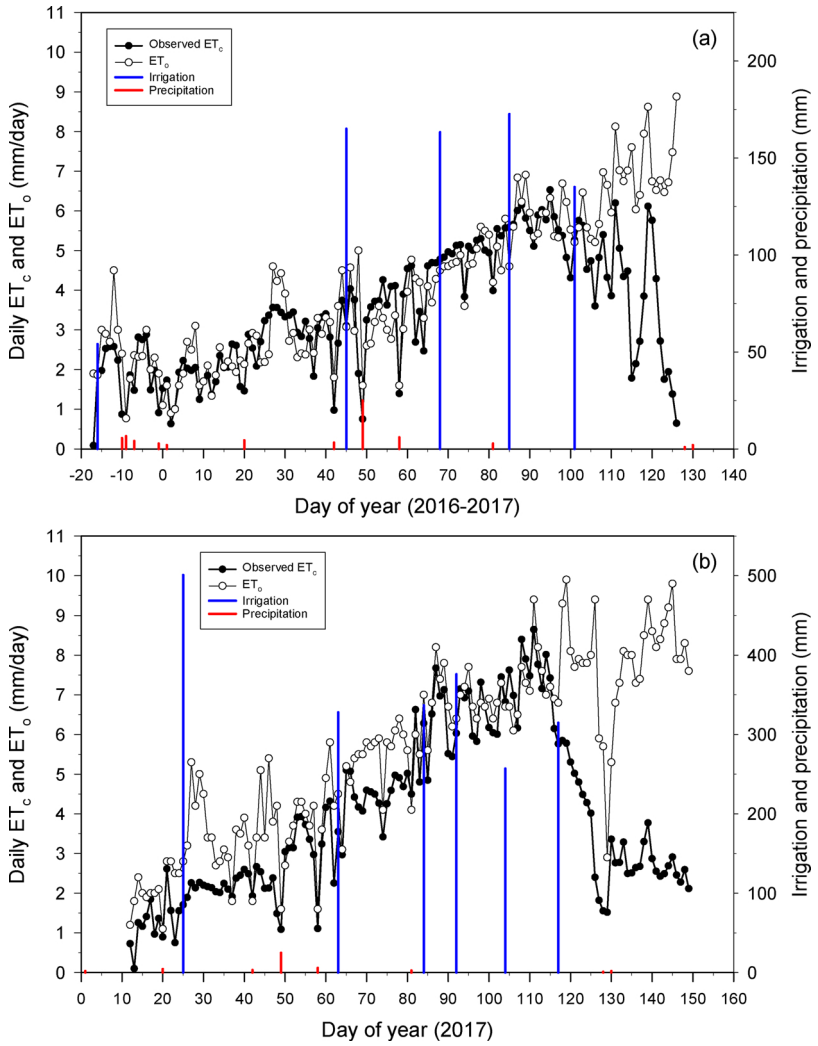

Fig. 4. Daily observed wheat evapotranspiration (ET_c) and measured irrigation depths at S8 (a) and J118 (b) and daily reference evapotranspiration (ET_o) and precipitation recorded at the Yuma North Gila AZMET weather station in 2016-17.

3.2. Satellite-based NDVI time series

NDVI over wheat showed patterns similar to observed ET_c, with a nearly flat trend before emergence, a rapid increase close to maximum values at DOY 50–60, a 30-day plateau region, then an abrupt 10 − 20-day NDVI decline on senescence. However, there were significant differences between fields when examining details. In 2017, S8′s earlier and more vigorous plant growth showed NDVI values rising above 0.8 and remaining above the later-planted J118 site until April (Fig. 7; dashed lines indicate threshold NDVI values for each site). The different planting dates of fields at S1-6 are readily apparent for the 2018 sites (Fig. 8). For these fields, irrigation cut-off led to nearly simultaneous senescence and nearly simultaneous NDVI drops. The range for non-atmospherically corrected values are compressed values, ranging 0.1 − 0.82. For the 2019 H8 site (Fig. 9), all 8 borders closely tracked each other, with NDVI ranging from 0.0 to 0.9, a result of using atmospherically corrected observations. Highlighted by the dashed lines is an interval of crop water stress that is represented by an NDVI drop of about 5%. The persistence of clear skies in combination with soil water balance modeling (discussed below) supports this interpretation.

3.3. Daily observed ET_c vs. estimated T_c and $ET_{c\ act}$

Applying the NDVI to K_{cb} transformations resulted in time-series modeled T_c (Yuma sites) and ET_c (Maricopa site) values that closely track observed ET_c for 2017 (Fig. 10a and 10b), for 2018 (Fig. 11a to 11d for Yuma sites) and 2019 (Fig. 12 for H8 in Maricopa). Trends previously observed are mimicked by NDVI-implemented modeling where many of the irrigation events are represented by spikes in both ET_c and satellite-based NDVI. The H8 site for 2019 shows the average modeled $ET_{c\ act}$ of the 8 borders along with observed ET_c at H8 (Fig. 12).

Results from estimated T_c and ET_c for the 2018 and 2019 seasons showed seasonal patterns, where VI-derived estimates closely agreed with observed ET_c at mid-season, but consistently underestimated ET_c at early and late growth seasons. Estimated T_c (non-adjusted for water stress) for early season conditions at Yuma sites in 2017 (Fig. 10) and 2018 (Fig. 11) are consistent with expectations: for sparse cover, T_c is low, while ET_c is relatively high due to soil evaporation. Observed ET_c for all four S sites in 2018 increased above estimated T_c following irrigations applied on day of year (DOY) 40 for S1 and S2 (Fig. 11a and b), DOY 30 for S5 (Fig. 11c), and DOY 53 for S6 (Fig. 11d). Starting in early March 2018, consistency among all four sites is restored. About DOY 65, at near full cover, and when T_c and ET_c should be nearly the same, estimated T_c agrees well with measured ET_c. During the later season (DOY after 110), T_c underestimates measured ET_c, suggesting higher soil evaporation at late-season irrigation when crop cover is reduced. For 2017, seasonal total estimated T_c is within 20 mm of total observed ET_c at S8 but was 73 mm less for J118 (Table 10). Seasonal total estimated T_c for Yuma site S2 is close (within 16 mm) to total

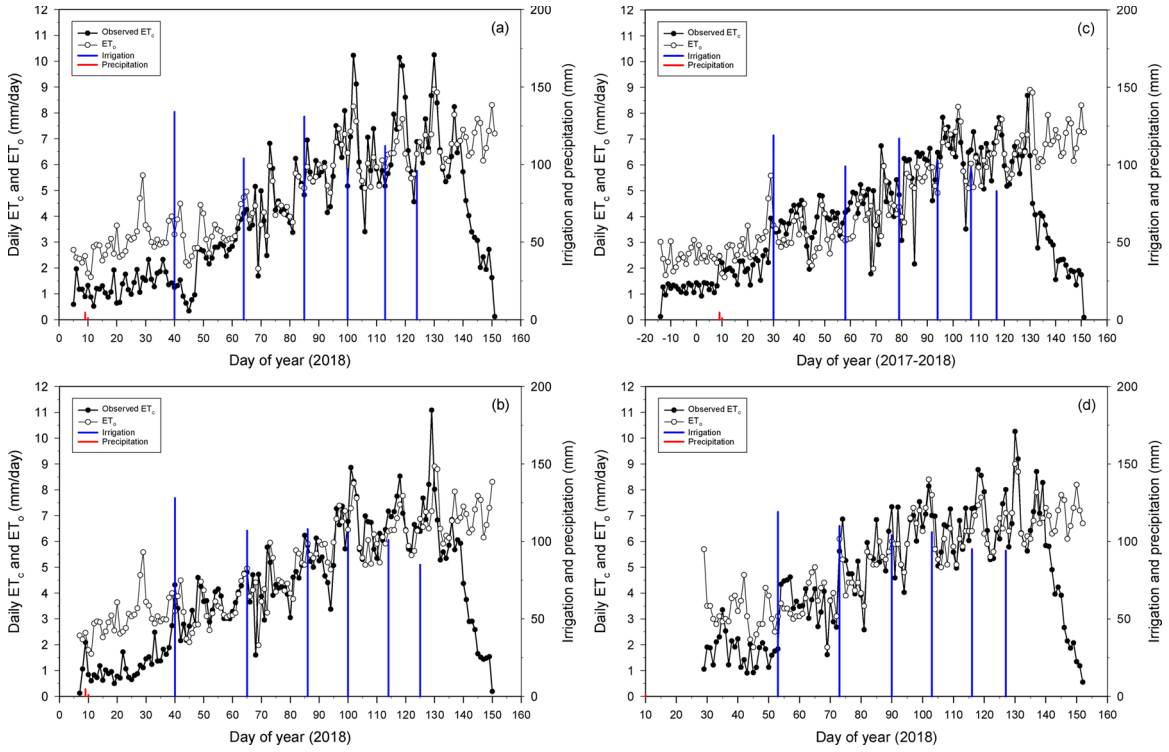

Fig. 5. Daily observed wheat evapotranspiration (ET_c) and measured irrigation depths at S1 (a), S2 (b), S5 (c), and S6 (d) and daily reference evapotranspiration (ET_o) and precipitation recorded at the Yuma North Gila AZMET weather station in 2017-18.

observed ET_c. However, for sites S1, S5, and S6, total T_c is 52–110 mm less than total observed ET_c, suggesting more soil evaporation may have occurred at those sites, particularly during the early season. At the Maricopa field (Fig. 12), where $ET_{c\ act}$ was estimated, agreement was very good except for underestimated ET_c for DOY between 20 and 35. Total estimated $ET_{c\ act}$ was only 17 mm less than observed total at H8. As alluded to earlier concerning water stress at H8, according to the SWB model the estimated $ET_{c\ act}$ was reduced by water stress ($K_s < 1.0$) for ten days at the end of a 21-day lapse without irrigation or significant rain (i.e., from DOY 98–107). This period is mid-season when wheat ET_c

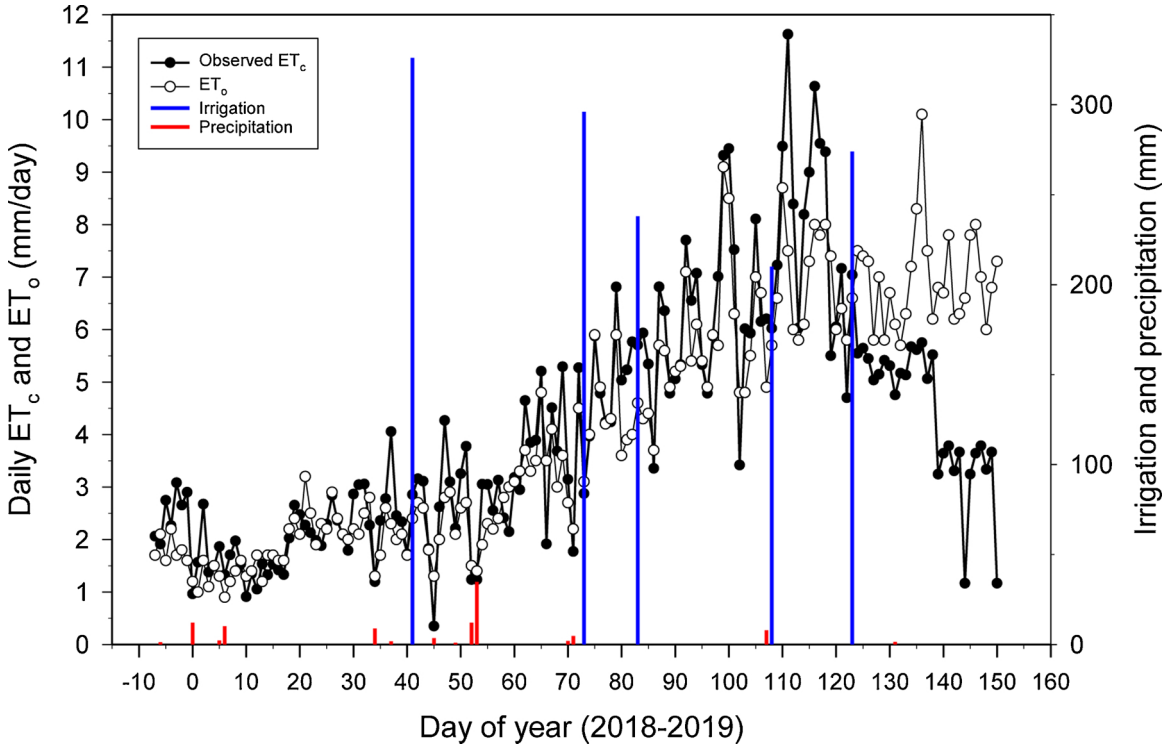

Fig. 6. Daily observed wheat evapotranspiration (ET_c) and measured irrigation depths measured at H8 and daily reference evapotranspiration (ET_o) and precipitation recorded at the Maricopa Agricultural AZMET weather station in 2018-19.

Table 10
Number of irrigations applied (N), total irrigation applied, total observed crop evapotranspiration (ET_c) from eddy covariance, total estimated crop transpiration (T_c) for Yuma sites: S1, S2, S5, S6, S8, and J118, total estimated ET_c for H8 (Maricopa), and grain yields for the seven durum wheat field sites in Arizona.

Site	Year	Irrigations*	Total irrigation applied (mm)	Total measured ET_c (mm)	Total estimated T_c or ET_c† (mm)	Grain yield (kg/ha)
S8	2016-17	5	690	499	479	6950
J118	2017	6	2114	540	467	5020
S1	2018	6	675	684	574	8070
S2	2018	6	635	588	572	8290
S5	2017-18	6	618	652	594	10180
S6	2018	6	627	578	526	7080
H8	2018-19	6	1710	635	618	6810

* Number of post planting irrigations.
† Tc estimated for all sites except H8.

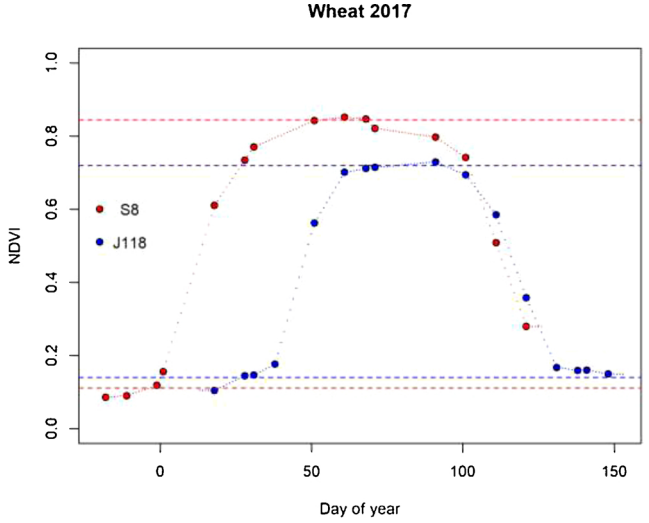

Fig. 7. NDVI time series for 2017 wheat sites S8 and J118 in Yuma. Sentinel 2 top-of-atmosphere observations indicated as solid circles. Dotted lines indicate interpolated NDVI. Dashed lines represent NDVI lower and upper limits as computed by 10% and 90% probability levels.

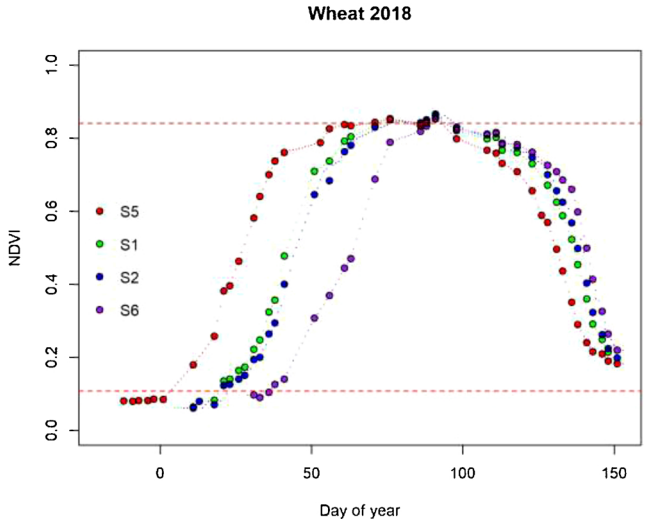

Fig. 8. NDVI time series for 2018 wheat sites S1, S2, S5, and S6 in Yuma. Sentinel 2 top-of-atmosphere observations indicated as solid circles. Dotted lines indicate interpolated NDVI. Dashed lines represent NDVI lower and upper limits for S5, computed by 10% and 90% probability levels. Limits for the other sites are not shown to maintain figure clarity but were similar to S5 values.

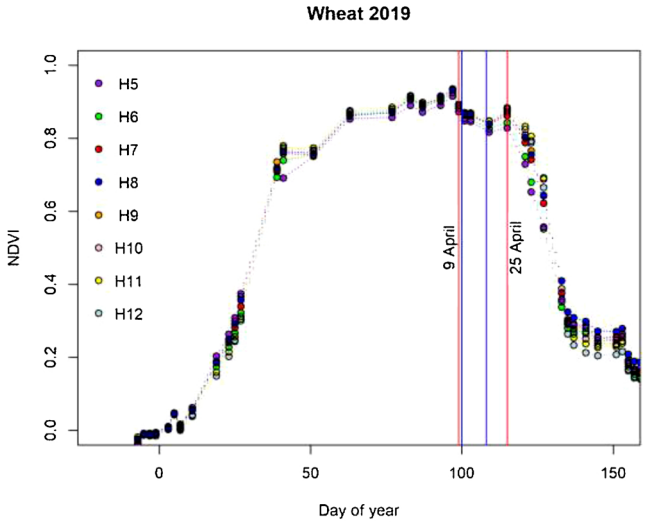

Fig. 9. NDVI time series for 2019 wheat site H8 in Maricopa, borders 5-12, derived from Eq. (3). Atmospherically corrected Venus observations indicated as solid circles. Dotted lines indicate interpolated NDVI. Red vertical lines denote the water stress interval as detected by Venus NDVI. Blue lines denote the onset and end of water stress as based on soil moisture depletion model. (For interpretation of the references to color in this figure legend, the reader is referred to the web version of this article.)

is high. The estimated water stress during this period reduced the estimated ET_c by about 17 mm from a non-stress condition. While observed ET_c also declined during this 10-day period, reduction was greater for $ET_{c\ act}$ (Fig. 12).

The statistical correlations and mean differences between daily estimated T_c or ET_c and the observed ET_c for different growth stages and for all stages combined are shown for the 2017 Yuma sites (Table 11) and for the 2018 sites in Yuma and the 2019 site in Maricopa (Table 12). The 2017 results indicate that estimated daily T_c was less than observed ET_c during initial-development stages with a MADP of 37–39%. As expected, based on the daily estimated and observed values shown in Fig. 10, agreement at S8 and J118 was much better during the mid-season stage (MADP within 14%), although mean T_c was higher than observed mean ET_c for S8. The trend remained for S8 during the late-season, suggesting observed ET_c may have experienced water-stress that was unaccounted for by the T_c estimates based on rather large gaps in NDVI data. For 2018, observed data were well-correlated (high r value and RMSE < 0.45 mm/d) for S1, S2, and S5 during the initial-development period, and less-correlated for S6 and H8. The higher correlations indicate that the daily trends for estimated T_c were similar to those for observed ET_c during the early growth stages, though mean daily T_c was much lower than mean observed ET_c, as indicated by the MADP (36–40%) for S1, S2, and S5. Although the estimated T_c (for S6) and $ET_{c\ act}$ (for H8) were not as well correlated with daily observed during the early growth stages, the MADP was about the same for S6 and even lower for H8 (28%) compared with the three other S sites. Smaller r values and higher RMSE during mid-season than early season for the four S sites indicate that daily values of estimated T_c were generally less aligned with daily observed fluctuations. Daily $ET_{c\ act}$ and observed ET_c were better correlated during mid-season than during earlier stages. For all sites, the absolute differences between estimated and observed were smallest during the mid-season, varying in MADP from 13% to 18% (Tables 11 and 12). Late-season r values were relatively high at all sites, indicating an agreement in trend between estimated and observed the daily values. Absolute agreement based on MADP (19–22%) was best for S5 and for the H8 site when $ET_{c\ act}$ was estimated. Considering the daily data for the entire season, estimated data were well-correlated and similar for all sites and years, where r values were 0.85–91 and RMSE were near 1.0 mm/d. Mean absolute

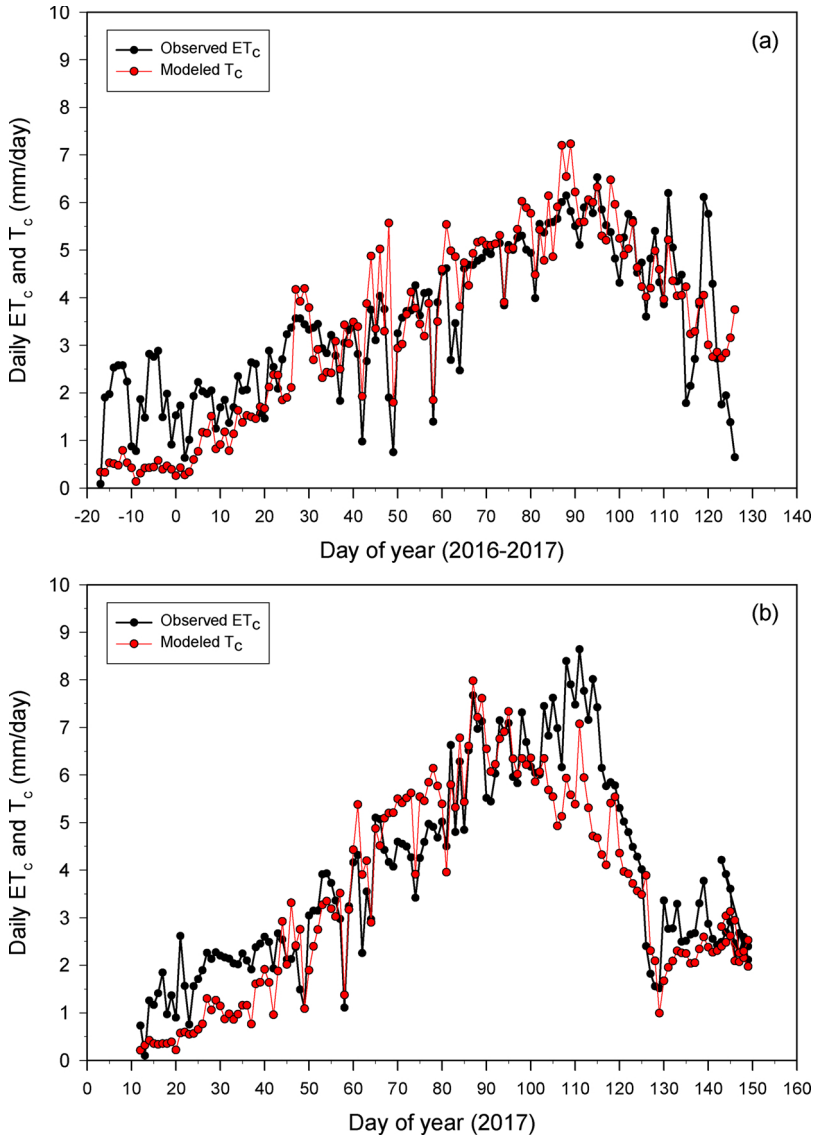

Fig. 10. Daily observed wheat evapotranspiration (ET_c) and daily estimated wheat crop transpiration (T_c) modeled as daily basal crop coefficient (K_{cb}), derived by normalized satellite NDVI, times the daily reference evapotranspiration (ET_o) at Yuma sites S8 (a) and J118(b).

differences for the entire season were from 0.78 to 1.07 mm/d, indicating estimated values were about 20–23% less than observed for the season.

The total irrigation applied to wheat borders at the six Yuma sites (Table 10) were generally not much higher than the total observed ET_c, albeit with one exception at J118., Otherwise, total irrigation varied from 34 mm less to 191 mm more than total ET_c, indicating high irrigation efficiencies. In contrast to these, irrigation at the Maricopa H8 site was less efficient, with total irrigation exceeding total ET_c by over 1000 mm. The grower at H8 realized something had changed in his organic wheat borders that made the water advance times much slower than in the previous year. The lowest grain yield for all sites was at J118 in 2017 (Table 10), which was a smaller field with a much sandier soil profile below 0.15 m than the other sites. Because of the high infiltration rate in J118, the field had to be irrigated at high flow rates, which ultimately led to exceedingly high irrigation depths relative to ET_c. The relatively low yield for H8 (organic wheat) could reflect deep leaching of nutrients due to excessive irrigation.

3.4. Daily observed K_c and modeled k_{cb} and K_c

High observed K_c during early-season for S8 in 2016–2017 (Fig. 13a) reflects soil evaporation due to the post-plant irrigation and the frequent occurrence of precipitation during Dec.-Jan. In contrast, J118 planted in mid-Jan. 2017 without a post-plant irrigation had lower observed K_c during the early stages of growth (Fig. 13b). At mid-season, average K_c at S8 was 1.06 but observed K_c likely declined during mid-season between DOY 77–84 due to water-stress. In contrast, average K_c during mid-season for J118 was only 0.92 and daily values were similar to modeled K_{cb} until DOY 100 when K_{cb} rapidly declined relative to observed K_c. End-of-season observed K_c was similar for S8 and J118, about 0.30. The measured K_c for the S1, S2, S5, and S6 Yuma sites in 2018 showed similar trends with time (Fig. 14). However, the measured K_c data during the early season for these sites were variable with generally lower observed K_c at the S1 site (Fig. 14a) and S2 site (Fig. 14b) than at S5 (Fig. 14c) and S6 (Fig. 14d). For all the S sites in 2018, except S6, which was planted later, K_c spikes high following a rain on DOY 9 and 10, albeit the two-day K_c spike in S5 appeared unrealistically high. For S6, the observed K_c spiked from DOY 55–60 following irrigation application. Although these spikes corresponded to a

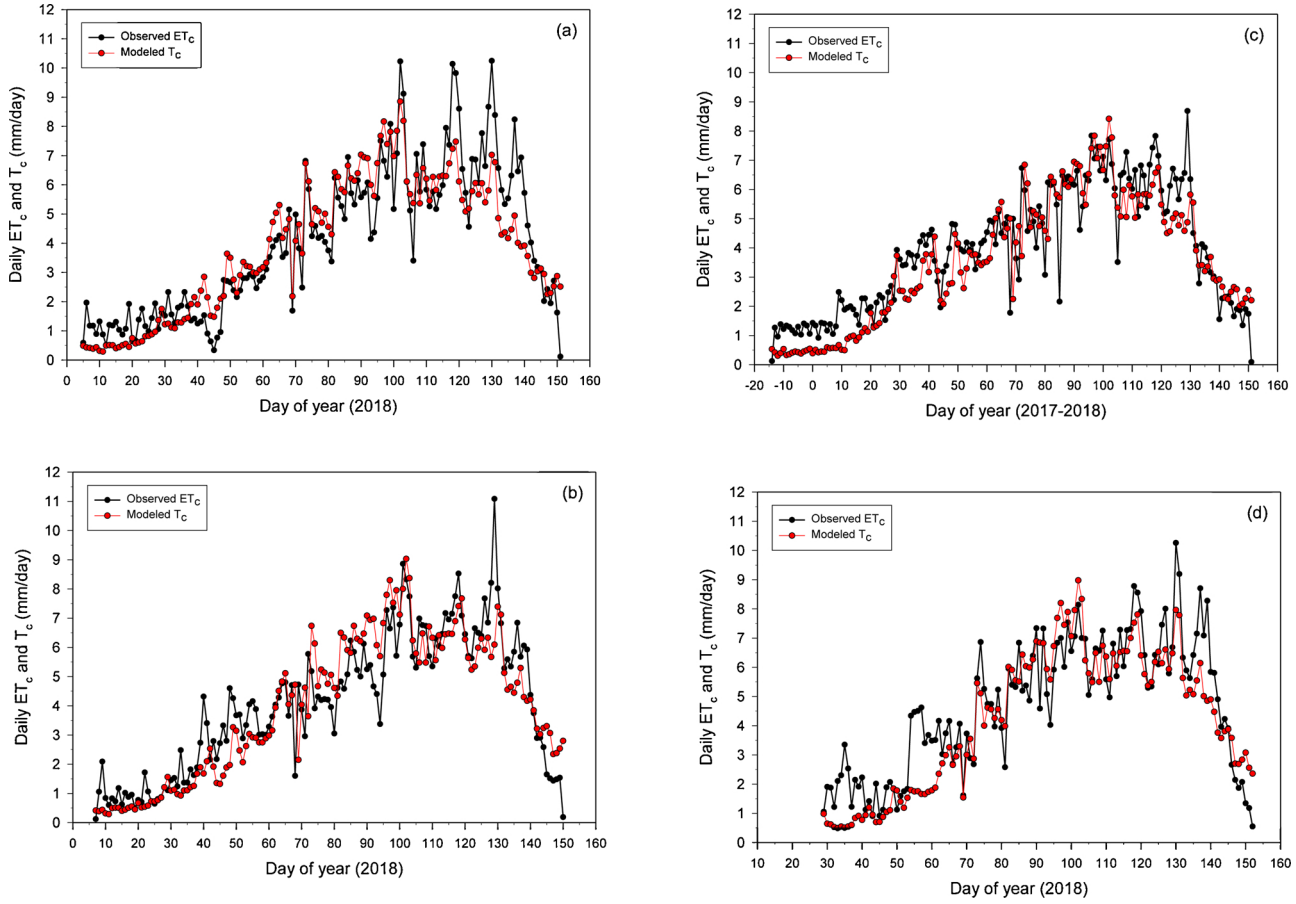

Fig. 11. Daily observed wheat evapotranspiration (ET_c) and daily estimated wheat crop transpiration (T_c) modeled as daily basal crop coefficient (K_{cb}), derived by normalized satellite NDVI, times the daily reference evapotranspiration (ET_o) at Yuma sites S1 (a), S2(b), S5 (c), and S6 (d) in 2017-18.

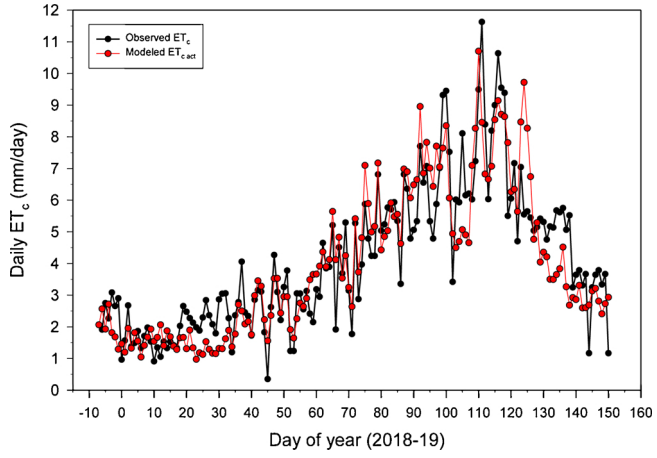

Fig. 12. Daily observed wheat evapotranspiration (ET_c) at H8 in Maricopa and daily estimated actual crop evapotranspiration ($ET_{c\ act}$) modeled using daily basal crop coefficients (K_{cb}) derived by normalized satellite NDVI, incorporated within the FAO56 dual crop coefficient procedures, and a simulated daily soil water balance of the crop root zone. Estimated $ET_{c\ act}$ represents the average of the eight borders at H8 in 2018-19.

time of low crop cover (indicated by the low NDVI at the time for S6 in Fig. 8), they were higher than expected. Thus, fitting an FAO56 initial horizontal K_c was difficult due to the variable early season K_c data. Measured K_c reached maximum values at mid-season from about DOY 40–70 depending on planting date for S sites and then K_c plateaued, fluctuating about the fitted horizontal mid-season FAO56 curve (Fig. 14). Obvious declines in K_c data occurred after mid-season, starting around DOY 130–140 for S1, S2, and S6 and around DOY 120 for S5, which was planted earlier than the other S sites. The K_c data at the estimated mid-season growth averaged 1.14 for S1, 1.05 for S2 and S6, and 1.10 for S5. Those values are the same as the estimated FAO56 mid-season segment shown in each figure. End of season K_c varied from about 0.20 to 0.30 for the S sites, indicating the dry soil condition prior to harvest. Estimated K_{cb} values derived from satellite NDVI show some overestimation from DOY 40–90 and underestimation after DOY 110, relative to the K_c for S1 (Fig. 14a). The estimated K_{cb} for S2 (Fig. 14b) appears to be closely representative of actual K_c data during development where K_{cb} is about 0.10 lower than K_c, though K_{cb} then becomes higher than K_c for a period during mid-season. The estimated K_{cb} values are much lower than K_c during initial through development stages for S5 and S6, likely indicating that soil evaporation was higher at those sites than S1 and S2. During mid-season and late, estimated K_{cb} is consistent with measured K_c for S5. For S6, mid-season K_{cb} fits the measured data well with some underestimation during late season. Comparison of the seasonal totals of measured ET_c show good agreement with the estimated total T_c (Table 10) for the S sites in 2018, showing total T_c was less than ET_c by 16–110 mm, depending on site.

For the Maricopa site (Fig. 15), an initial FAO56 K_c line was not given due to very high early season measured K_c caused by significant rain during January 2019. The K_c during development period (DOY 10–50) for H8 was also skewed when frequent rain occurred. The estimated FAO56 mid-season K_c for H8 in 2019 was 1.1, higher than those in Yuma in 2018. The end of season K_c was about 0.40. The SWB and VI-based modeled daily K_c was not consistent with observed K_c during the rainy development period. However, it was close to the observed data during mid-season. The modeled K_c captured the decline in K_c due

Table 11
Summary statistics for observed crop evapotranspiration (ET_c) and estimated crop transpiration (T_c) for the S8 and J118 Yuma sites in 2017. Statistics used to evaluate differences between estimated and observed include mean, correlation coefficient (r), root mean square error (RMSE), mean difference (MD), mean absolute difference (MAD), and percent MAD (MADP) of mean observed.

Site	Wheat growth stage[a]	Mean crop T_c		Statistic				
		Observed (mm/d)	Estimated (mm/d)	r (-)	RMSE (mm/d)	MD (mm/d)	MAD (mm/d)	MADP (%)
S8	Initial-develop.	2.28	1.65	0.72	0.88	0.63	0.90	39.4
J118		2.19	1.60	0.80	0.72	0.59	0.82	37.4
S8	Mid-season	4.20	4.51	0.70	0.76	−0.31	0.59	14.0
J118		5.74	5.50	0.68	0.67	0.24	0.75	13.0
S8	Late-season	4.57	4.74	0.72	0.89	−0.17	0.80	17.4
J118		3.92	3.11	0.92	0.55	0.81	0.93	23.7
S8	All stages	3.47	3.33	0.85	1.02	0.14	0.78	22.6
J118		3.91	3.38	0.91	0.86	0.53	0.82	21.1

[a] Growth stages are approximate based on visually-fitted observed crop coefficient (K_c) curve over the season. All stages include data for the entire season.

Table 12
Summary statistics for observed crop evapotranspiration (ET_c) and estimated crop transpiration (T_c) for the S1, S2, S5, and S6 Yuma sites in 2018 and estimated actual ET_c for the H8 Maricopa site in 2019. Statistics used to evaluate differences between estimated and observed include mean, correlation coefficient (r), root mean square error (RMSE), mean difference (MD), mean absolute difference (MAD), and percent MAD (MADP) of mean observed.

Site	Wheat growth stage[a]	Mean crop ET_c or T_c		Statistic				
		Observed (mm/d)	Estimated (mm/d)	r (-)	RMSE (mm/d)	MD (mm/d)	MAD (mm/d)	MADP (%)
S1		2.17	1.33	0.90	0.41	0.83	0.85	39.2
S2		1.85	1.23	0.85	0.43	0.62	0.67	36.0
S5	Initial-develop.	2.08	1.28	0.90	0.45	0.80	0.85	40.8
S6		2.69	1.72	0.74	0.80	0.98	1.05	38.8
H8		2.18	1.85	0.54	0.55	0.33	0.60	27.7
S1		6.15	5.65	0.81	0.82	0.50	0.96	15.6
S2		5.35	5.67	0.73	1.06	−0.34	0.94	17.6
S5	Mid-season	5.05	5.02	0.68	1.15	0.02	0.60	17.9
S6		6.31	6.23	0.71	0.78	0.08	0.60	12.7
H8		4.86	5.09	0.83	0.96	−0.23	0.87	18.0
S1		5.26	3.89	0.92	0.55	1.37	1.92	36.4
S2		4.84	4.47	0.87	0.73	0.38	1.16	23.9
S5	Late-season	4.53	4.21	0.91	0.63	0.31	0.84	18.6
S6		3.72	3.60	0.95	0.29	0.12	1.18	31.8
H8		5.66	5.33	0.81	1.47	0.33	1.25	22.0
S1		4.65	3.90	0.89	1.03	0.75	1.07	23.1
S2		4.08	3.98	0.88	1.16	0.11	0.89	21.7
S5	All stages	3.93	3.58	0.88	1.02	0.35	0.87	22.1
S6		4.66	4.24	0.88	1.11	0.42	0.94	20.1
H8		4.09	3.97	0.88	1.09	0.12	0.87	21.4

[a] Growth stages are approximate based on visually-fitted observed crop coefficient (K_c) curve over the season. All stages include data for the entire season.

to water stress between DOY 98 and 107 and the increased jump in observed K_c following the irrigation on DOY 108. As mentioned earlier, total observed ET_c was 17 mm more than total modeled ET_c (Table 10) indicating good seasonal agreement. Estimated seasonal evaporation for H8 was about 65 mm, similar to the difference in total ET_c and T_c at the S5 and S6 sites.

3.5. Assessment of satellite-based NDVI

Lastly, a parallel study assessed the importance of atmospheric correction to satellite reflectance data and specifically to resulting ET estimates. As expected, NDVI values were found strongly affected, but subsequent effects were greatly reduced after NDVI normalization. Results from analysis over the H8 site at Maricopa are shown in Fig. 16a, and for the S wheat sites at Yuma in Fig. 16b. Red symbols represent parameters derived from non-corrected L1C Venus data, while blue symbols are corresponding parameters for corrected L2A data. The adjusted NDVI—denoted ACORVI on top panels—are sensitive to atmospheric corrections, where the range of indices are reduced by 25–40%. When the ACORVI values are normalized using Eq. (1) and VI limits at 10% and 90% quantiles, $NDVI_n$ estimates from L1C mostly agree within 5% of L2A data for both sites. Normalization at Yuma led to thresholding at full canopy, a contributing factor to the small differences observed at mid-season. Transformations to K_{cb} are shown in the third panels of Fig. 16a and 16b. At the Maricopa H 8 site, normalization thresholds for L1C data over-estimate surface reflectance in the early and mid-seasons, while the over-estimations occur in the late season for Yuma sites, a difference possibly due to differing soil reflectivity. Daily ET_c values, bottom-most panels, are obtained by linearly interpolating satellite derived K_{cb} values to daily time steps, then multiplying these by ET_o obtained from AZMET data. Daily ET_c estimates differ by less than 1 mm/day and cumulative full season ET (indicated on left side of each panel) by ~30 mm. This two-site test indicated that use of top-of-atmosphere satellite data, after normalization, is likely to result in ET_c estimation errors on the order of 5% or less.

4. Discussion

Results from the Arizona wheat studies demonstrated the

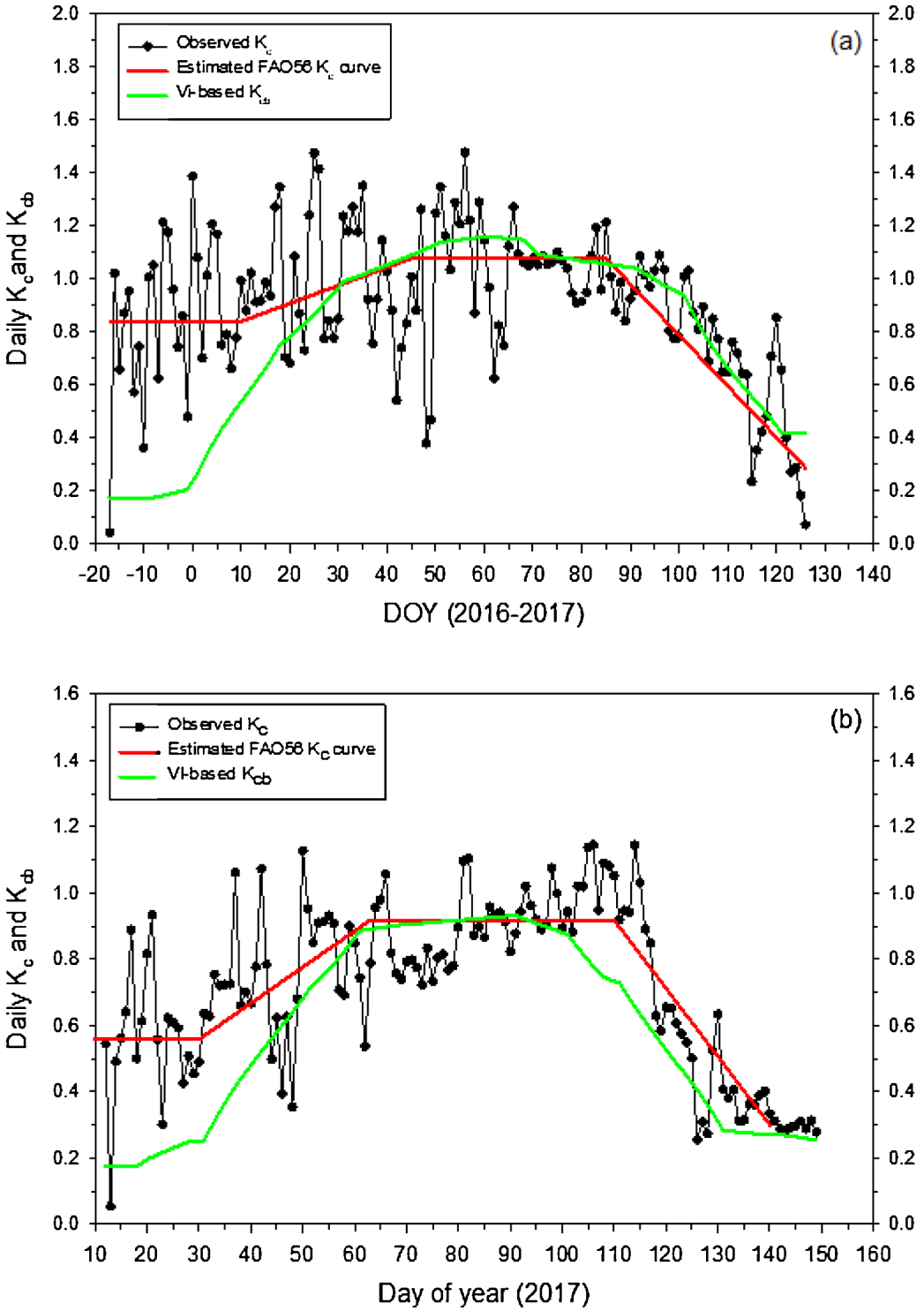

Fig. 13. Daily observed wheat single crop coefficient (K_c), FAO56 K_c curve visually fitted to observed data, and daily estimated basal crop coefficient (K_{cb}) derived from normalized satellite NDVI, assuming no water stress, for Yuma fields S8 (a), and J118 (b) in 2016-17.

practicality and accuracy of the spaceborne NDVI-based K_{cb} model to estimate daily and seasonal crop water use of wheat. Usable satellite scenes ranged between 25 and 65 per growing season, which corresponds to a realized periodicity of 3–7 days. This high cadence, possible because of Sentinel 2 and Venus capabilities and a favorable clear sky environment, enabled excellent tracking of wheat canopy growth. Considering 7 sites visited over 2016–2019 using eddy covariance observations, the study estimated total ET_c in the range of 499–684 mm, values less than total irrigation on the order of 50 − 100 mm for S1-S6 sites and 201 mm for S8, suggesting reasonable irrigation efficiencies at those sites. Notable exceptions in irrigation efficiency occurred at H8, where applied irrigations exceeded observed ET_c by over 1000 mm and J118, where irrigations exceeded ET_c by nearly 1500 mm. These differences highlight that EC monitoring generally cannot capture highly inefficient scheduling absent slow infiltration conditions. Comparing total observed ET_c for seven sites in Arizona to remotely sensed estimates showed agreement within 16–110 mm over the growing season, and estimates were consistent with the seasonal ET_c value of 655 mm

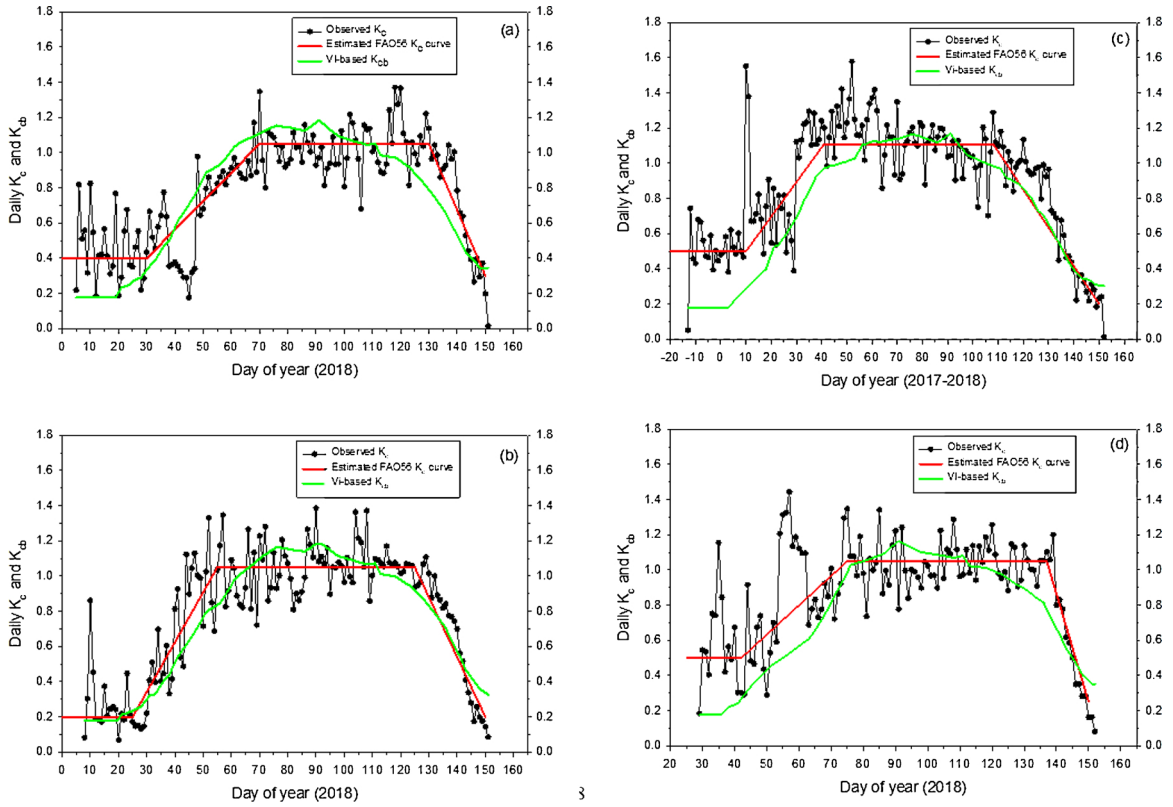

Fig. 14. Daily observed wheat single crop coefficient (K_c), FAO56 K_c curve visually fitted to observed data, and daily estimated basal crop coefficient (K_{cb}) derived from normalized satellite NDVI, assuming no water stress, for Yuma fields S1 (a), S2(b), S5 (c), and S6 (d) in 2017-18.

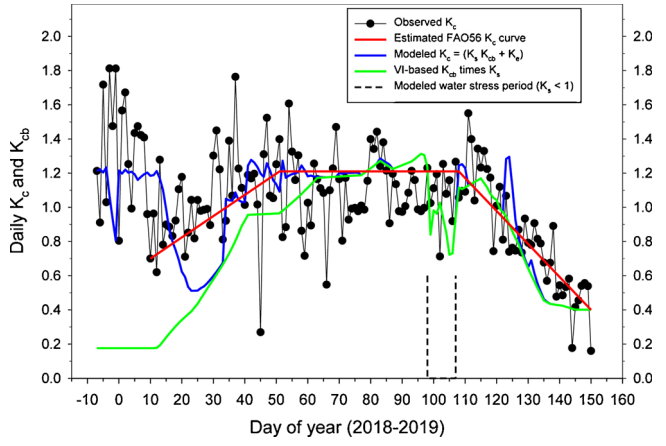

Fig. 15. Daily observed wheat single crop coefficient (K_c) at H8 in Maricopa, FAO56 K_c curve visually fitted to observed data, daily modeled K_c, based on estimated basal crop coefficients (K_{cb}), derived from normalized satellite NDVI and adjusted by the water stress coefficient (K_s), plus the estimated soil evaporation coefficient (K_e), calculated using FAO56 dual crop coefficient procedures and simulated daily soil water balance (SWB) of the crop root zone and soil evaporation layer. Modeled K_c and K_{cb} lines for H8 represent averages calculated separately for the eight borders in 2018-2019.

provided by Erie et al. (1982) for the Southwestern US. This indicates that satellite based VI offers a good way to estimate seasonal ET_c once relationships with EC data have been tested.

When assessing within season water use there were differences in performance of the VI-based estimates in early vs. mid-late periods. Mid-season observed K_c values ranged from 1.05 to 1.14 for sites that were considered not highly water-stressed and values are consistent with literature findings for wheat reported by Pereira et al. (2020, this Special Issue), which ranged from 1.0–1.3 based on the FAO56 grass reference ET_o. Observed end-of-season K_c varied from about 0.2 to 0.4 considering the Yuma and Maricopa sites. Range in values reported for end-of-season wheat K_c in the literature review by Pereira et al. (2020) are from 0.1 to 0.4 for low moisture grain. Agreement between T_c and ET_c estimates obtained via Sentinel 2 and Venus observations, respectively, agreed well with EC observations after the first 50–60 days of growth. On the other hand, early season T_c and ET_c estimates in 2016–2019 (< 60 days), were erratic and not as reliable, an outcome to be expected in part because sparse vegetation cover contributes a noisy and weak signal to the NDVI time series. Note that had an alternate linear formulation for K_{cb} been used (Drerup et al., 2017; Er-Raki et al., 2007), early season T_c and ET_c estimates would also be less than observed. Additional reasons for worse early season performance were the occurrences of soil surface evaporation from rainfall events and some EC sensor failures. Soil evaporation could be better accommodated with thermal remote sensing with sensors such as Landsat and ECOSTRESS. Errors induced by equipment failure emphasize the difficulty of data gap filling. Lacking sufficient thermal data, utilization of FAO56 methods (Allen et al., 1998) to estimate K_c remains preferred for the early season irrigation scheduling. This may also include the need to construct an appropriate localized segmented FAO56 K_c curve to estimate ET_c until satellite NDVI are deemed reliable (e.g., 60 days after planting, when irrigation scheduling starts in earnest in Arizona).

A notable finding from the study was a demonstration of the ability to use NDVI to detect water stress. Commonly one assumes that the NDVI signal is too imprecise to be used for abnormal plant water conditions, and for such cases thermal infrared sensing should be used. In a ground-based study over wheat, Jackson et al. (1982) reported no immediate resolution of water stress with any of the tested indices. Data from this study indicate that is not necessarily true. Results from the 2017 Yuma sites (S8 and J118) and the 2019 Maricopa H8 sites showed that for irrigated seasonal crops, such as wheat, a combination of

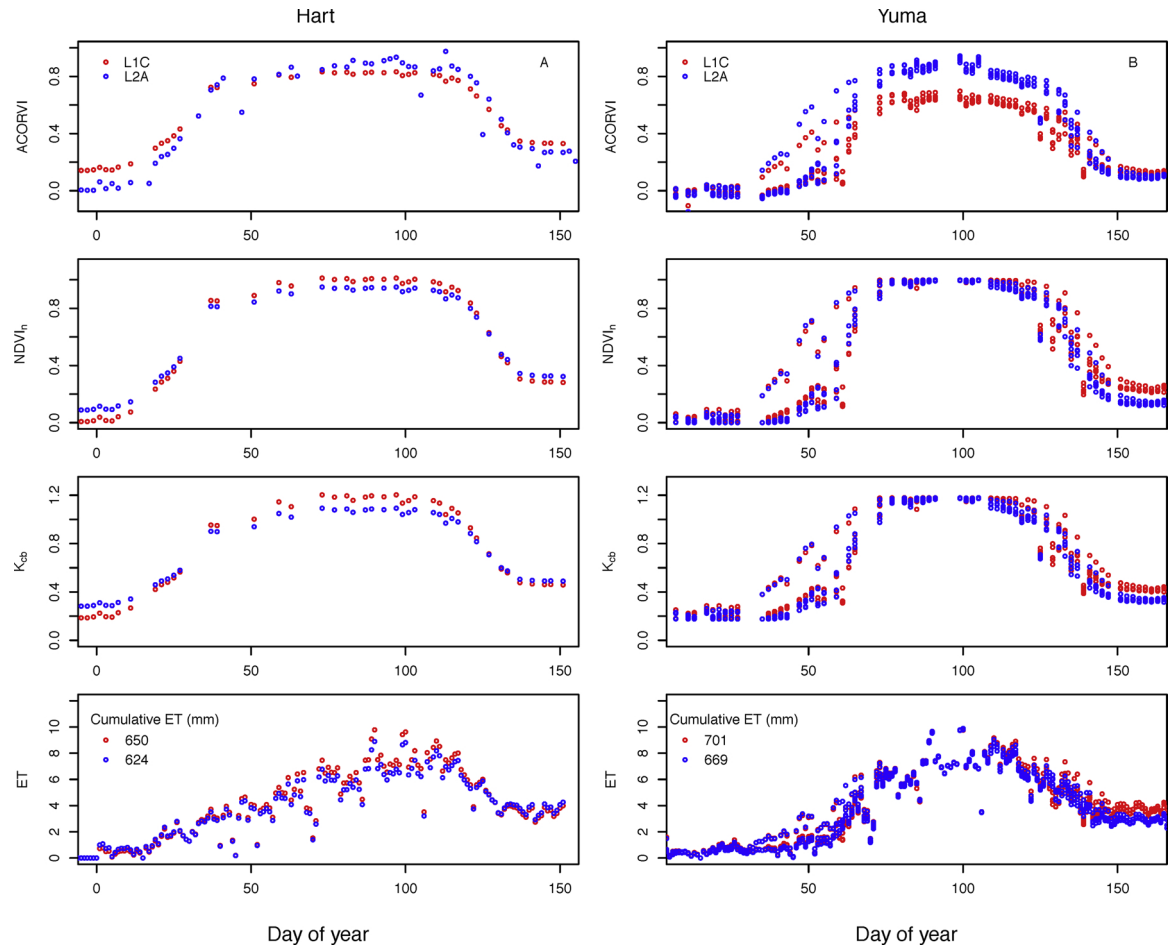

Fig. 16. VI sensitivities to atmospheric correction. Effects on ACORVI, $NDVI_n$, K_{cb}, and ET_c were evaluated over the Maricopa H8 site in (A) and 5 Yuma S sites (B) in 2019. Two Venus satellite data products were used for the comparisons: 5-m TOA L1C (red) and 10-m surface reflectance L2A (blue). While significant differences existed between the two products for ACORVI, differences after VI-normalization were generally reduced. Cumulative ET_c estimate differences were ~30 mm. (For interpretation of the references to color in this figure legend, the reader is referred to the web version of this article.)

frequent, well-calibrated, high spatial resolution visible near infrared remote sensing can resolve water stress. For the Maricopa event a clear and persistent 5% drop in NDVI occurred within 2 days of soil water balance model predicted stress. One can foresee an operational system with short latency that could detect and forecast water stress events based on a collection of frequent NDVI data supported by a background soil water balance model. Although the study did not investigate SWB status at the 2017 Yuma S8 and J118 sites, stress may be indicated there too by NDVI. In these instances, the indicators could be anomalous depressions at short- and long-duration time scales. Thus, for non-standard conditions, quantile selection for NDVI normalization won't be sufficient for crop coefficient estimation. Instead, historical or spatially contextual selection of NDVI limits would be needed. Required conditions to make detection feasible and reliable include accurate atmospheric corrections to the time series, accurate satellite calibration, similar satellite view angles for all overpasses, high spatial (10 m or better) resolution, and frequent overpasses (<7 days). This latter aspect, which Venus eminently provided with 2-day sampling, demonstrates the value of high cadence imaging. With frequent images, trend persistence adds confidence that the observations are real and not acquisitional or processing artifacts. Less frequent images, separated by a week or more, would make it more likely that stress signals would remain unrecognized because of small sample sizes and the increased probability of confounding rainfall or irrigation events. The availability of frequent images also suggests a change in analysis: time series should not be smoothed with filters such as Savitzky-Golay (Savitzky and Golay, 1964) because that step would reduce or remove the stress signals.

5. Conclusions

A three-year study was undertaken to evaluate and validate T_c and ET_c over irrigated durum wheat using a previously developed basal crop coefficient model based on vegetation indices that were derived in this study from spaceborne platforms. Comparisons based on eddy covariance ET_c observations indicated the remotely sensed modeled values agreed very well for the total season and for most of the growing season, with best agreement during mid-season. Measured single crop coefficients at mid-season and end of season for durum wheat were consistent to those presented in the original FAO56 table and to those updated in the present Special Issue. Agreement was not as good for early season wheat growth, an outcome consistent with the limited ability of VIs to detect soil evaporation and to accurately represent transpiration over sparse cover. The latter results suggest that additional methods, such as FAO56 procedures to handle initial K_c values, or additional measurements will be needed to supplement VI-based ET_c capabilities prior to effective wheat cover. However, mid-season ET_c can be accurately modeled with VI-based approaches, even during water stress events. The results strengthen existing reports on FAO56 mid-season crop coefficients to use for wheat. Additional studies in environments different from the U.S. Southwest are needed to show that the VI methodology is broadly applicable for wheat grown

elsewhere. In addition, the satellite-based approach described in this study is under evaluation for lettuce, spinach, melon, and cotton. The aim is to demonstrate its potential for ET estimation accuracy and practicality to become a routine decision support tool for crop water management.

Declaration of Competing Interest

The authors declare that they have no known competing financial interests or personal relationships that could have appeared to influence the work reported in this paper.

Acknowledgements

Major support for all Yuma activities was provided by the U.S. Bureau of Reclamation under R16PG00152, Arizona Grain Research and Promotion Council under AGRPC 18-05, NASA NNH17AE42I, NASA/JPL 1616792, and by the University of Arizona's Yuma Center of Excellence for Desert Agriculture (YCEDA). Special thanks to D. Drewry & G. Rivera, NASA/JPL and M. Tuller, University of Arizona, for loan of eddy covariance stations. Remote sensing results would not have been possible without Sentinel 2 provided by the European Space Agency, and Venus, provided by Centre National d'Etudes Spatiales (CNES, France) and Israel Space Agency (ISA).

Appendix A. Supplementary data

Supplementary material related to this article can be found, in the online version, at doi:https://doi.org/10.1016/j.agwat.2020.106266.

References

Allen, R.G., Pereira, L.S., Raes, D., Smith, M., 1998. Crop Evapotranspiration. FAO Irrigation and Drainage Paper 56. Food and Agric. Org. of the United Nations, Rome, Italy.

Anderson, R.G., Wang, D., 2014. Energy budget closure observed in paired Eddy Covariance towers with increased and continuous daily turbulence. Agric. For. Met. 184, 204–209.

Bausch, W.C., 1995. Remote sensing of crop coefficients for improving the irrigation scheduling of corn. Agric. Water Manag. 27, 55–68.

Bausch, W.C., Neale, C.M.U., 1989. Crop coefficients derived from reflected canopy radiation: a concept. Trans. ASAE 30, 703–709.

Campos, I., Neale, C.M.U., Calera, A., Balbontín, C., González-Piqueras, J., 2010. Assessing satellite-based basal crop coefficients for irrigated grapes (Vitis vinifera L.). Agric. Water Manag. 98, 45–54.

Drerup, P., Brueck, H., Scherer, H.W., 2017. Evapotranspiration of winter wheat estimated with the FAO 56 approach and NDVI measurements in a temperate humid climate of NW Europe. Agric. Water Manag. 192, 180–188.

Duchemin, B., Hadria, R., Er-Raki, S., Boulet, G., Maisongrande, P., Chehbouni, A., Escadafal, R., Ezzahar, J., Hoedjes, J.C.B., Kharrou, M.H., Khabba, S., Mougenot, B., Olioso, A., Rodriguez, J.C., Simonneaux, V., 2006. Monitoring wheat phenology and irrigation in Central Morocco: on the use of relationships between evapotranspiration, crops coefficients, leaf area index and remotely sensed vegetation indices. Agric. Water Manag. 79, 1–27.

Erie, L.J., French, O.F., Bucks, D.A., Harris, K., 1982. Consumptive Use of Water by Major Crops in the Southwestern United States. USDA-ARS Conservation Research Report Number 29.

Er-Raki, S., Chehbouni, A., Guemouria, N., Duchemin, B., Ezzahar, J., Hadria, R., 2007. Combining FAO-56 model and ground-based remote sensing to estimate water consumptions of wheat crops in a semi-arid region. Agric. Water Manag. 87, 41–54.

Er-Raki, S., Chehbouni, A., Boulet, G., Williams, D.G., 2010. Using the dual approach of FAO-56 for partitioning ET into soil and plant components for olive orchards in a semi-arid region. Agric. Water Manag. 97, 1769–1778.

French, A.N., Hunsaker, D.J., Bounoua, L., Karnieli, A., Luckett, W.E., Strand, R., 2018. Remote sensing of evapotranspiration over the central Arizona irrigation and drainage district, USA. Agronomy 8, 278.

Glenn, E., Neale, C., Hunsaker, D.J., Nagler, P., 2011. Vegetation index-based crop coefficients to estimate evapotranspiration by remote sensing in agricultural and natural ecosystems. Hydrol. Processes 25, 4050–4062.

González-Dugo, M.P., Mateos, L., 2008. Spectral vegetation indices for benchmarking water productivity of irrigated cotton and sugarbeet crops. Agric. Water Manag. 95, 48–58.

Gonzalez-Dugo, M.P., Neale, C.M.U., Mateos, L., Kustas, W.P., Prueger, J.H., Anderson, M.C., Li, F., 2009. A comparison of operation remote sensing-based models for estimating crop evapotranspiration. Agric. For. Met. 149, 1843–1853.

Hagolle, O., Huc, M., Villa Pascual, D., Dedieu, G., 2015. A multi-temporal and multi-spectral method to estimate aerosol optical thickness over land, for the atmospheric correction of FormoSat-2, LandSat, VENuS and Sentinel-2 images. Remote Sens. 7, 2668–2691.

Huete, A.R., 1988. A soil – adjusted vegetation index (SAVI). Remote Sens. Environ. 25, 295–309.

Hunsaker, D.J., Pinter Jr, P.J., Kimball, B.A., 2003. Estimating cotton evapotranspiration crop coefficients with a multispectral vegetation index. Irrig. Sci. 22, 95–104.

Hunsaker, D.J., Barnes, E.M., Clarke, T.R., Fitzgerald, G.J., Pinter Jr., P.J., 2005a. Cotton irrigation scheduling using remotely sensed and FAO-56 basal crop coefficients. Trans. ASAE 48 (4), 1395–1407.

Hunsaker, D.J., Pinter, P.J., Kimball, B.A., 2005b. Wheat basal crop coefficients determined by normalized difference vegetation index. Irrig. Sci. 24, 1–14.

Hunsaker, D.J., Fitzgerald, G.J., French, A.N., Clarke, T.R., Ottman, M.J., Pinter Jr, P.J., 2007. Wheat irrigation management using multispectral crop coefficients: I. Crop evapotranspiration prediction. Trans. ASABE 50, 2017–2033.

Jackson, R.D., Idso, S.B., Reginato, R.J., Pinter Jr, P.J., 1980. Remotely sensed crop temperatures and reflectances as inputs to irrigation scheduling. Irrigation and Drainage Special Conference Proceedings, 23–25 July. ASCE, New York, Boise, Idaho, pp. 390–397.

Jackson, R.D., Slater, P.N., Pinter Jr, P.J., 1982. Discrimination of Growth and Water Stress in Wheat by Various Vegetation Indices Through a Clear and Turbid Atmosphere. Early Warning and Crop Condition Assessment. AgRISTARS, NASA.

Jayanthi, H., Neale, C.M.U., Wright, J.L., 2007. Development and validation of canopy reflectance-based crop coefficient for potato. Agric. Water Manag. 88, 235–246.

Kabbaj, H., Sall, A.T., Al-Abdallat, A., Geleta, M., Amri, A., Filali-Maltouf, A., Belkadi, B., Ortiz, R., Bassi, F.M., 2017. Genetic diversity within a global panel of durum wheat (Triticum durum) landraces and modern germplasm reveals the history of alleles exchange. Front. Plant Sci. 8 (1277), 1–13.

Moffat, A.M., Papale, D., Reichstein, M., Hollinger, D.Y., Richardson, A.D., Barr, A.G., Beckstein, C., Braswell, B.H., Churkina, G., Desai, A.R., Falge, E.M., Gove, J.H., Heimann, M., Hui, D., Jarvis, A.J., Kattge, J., Noormets, A., Stauch, V.J., 2007. Comprehensive comparison of gap-filling techniques for eddy covariance net carbon fluxes. Agric. For. Met. 147, 209–239.

Mon, J., Bronson, K.F., Hunsaker, D.J., Thorp, K.R., White, J.W., French, A.N., 2016. Interactive effects of nitrogen fertilization and irrigation on grain yield, canopy temperature, and nitrogen use efficiency in overhead sprinkler-irrigated durum wheat. Field Crops Res. 191, 54–65.

Neale, C.M.U., Bausch, W.C., Heermann, D.F., 1989. Development of reflectance-based crop coeffcients for corn. Trans. ASAE 32, 1891–1899.

Pereira, L.S., Paredes, P., Hunsaker, D.J., López-Urrea, R., Mohammadi Shad, Z., 2020. Standard single and basal crop coefficients for field crops. Updates and advances to the FAO56 crop water requirements method. Agric. Water Manag this Special Issue.

Pinter Jr, P.J., Hatfield, J.L., Schepers, J.S., Barnes, E.M., Moran, M.S., Daughtry, C.S., Upchurch, D.R., 2003. Remote sensing for crop management. Photogramm. Eng. Remote Sens. 69 (6), 647–664.

Pôças, I., Calera, A., Campos, I., Cunha, M., 2020. Remote sensing for estimating and mapping single and basal crop coefficients: a review on spectral vegetation indices approaches. Agric. Water Manag this Special Issue.

Rozenstein, O., Haymann, N., Kaplan, G., Tanny, J., 2018. Estimating cotton water consumption using a time series of Sentinel-2 imagery. Agric. Water Manag. 207, 44–52.

Sánchez, N., Martínez-Fernández, J., González-Piqueras, J., González-Dugo, M.P., Baroncini-Turrichia, G., Torres, E., Calera, A., Pérez-Gutiérrez, C., 2012. Water balance at plot scale for soil moisture estimation using vegetation parameters. Agric. For. Met 166–167, 1–9.

Savitzky, A., Golay, M.J.E., 1964. Smoothing and differentiation of data by simplified least squares procedures. Anal. Chem. 36 (8), 1627–1639.

Taylor, R.D., Koo, W.W., 2015. 2015 outlook of the U.S. And world wheat industries, 2015-2024. Agribus. Appl. Econ. 738, 1–23.

Transon, J., Andrimont, R., Maugnard, A., Defourny, P., 2018. Survey of hyperspectral earth observation applications from space in the Sentinel-2 context. Remote Sens. 10 (157), 1–32.

Twine, T.E., Kustas, W.P., Norman, J.M., Cook, D.R., Houser, P.R., Meyers, T.P., et al., 2000. Correcting eddy-covariance underestimates over a grassland. Agric. For. Met. 103, 279–300.

Vickers, D., Mahrt, L., 1996. Quality control and flux sampling problem for tower and aircraft data. J. Atmos. Ocean Technol. 14, 512–526.

Webb, E.K., Pearman, G.I., Leuning, R., 1980. Correction of flux measurements for density effects due to heat and water vapour transfer. Q. J. R. Meteorol. Soc. 106, 85–100.

Wiegand, C.L., Richardson, A.J., Escobar, D.E., Gerbermann, A.H., 1991. Vegetation indices in crop assessment. Remote Sens. Environ. 35, 105–119.